Parallelizable Global Quasi-Conformal Parameterization of Multiply Connected Surfaces via Partial Welding*

Zhipeng Zhu[†], Gary P. T. Choi[‡], and Lok Ming Lui[†]

Abstract. Conformal and quasi-conformal mappings have widespread applications in imaging science, computer vision, and computer graphics and can be used in surface registration, segmentation, remeshing, and texture map compression. While various conformal and quasi-conformal parameterization methods for simply connected surfaces have been proposed, efficient parameterization algorithms for multiply connected surfaces have been less explored. In this paper, we propose a novel parallelizable algorithm for computing the global conformal and quasi-conformal parameterizations of multiply connected surfaces onto a 2D circular domain using variants of the partial welding method and the Koebe's iteration. The main idea is to first partition a multiply connected surface into several subdomains and compute the free-boundary conformal and quasi-conformal parameterizations of them, respectively, and then apply a variant of the partial welding algorithm to reconstruct the global mapping. We apply the Koebe's iteration, together with the geodesic algorithm, to the boundary points and welding paths before and after the global welding to transform all the boundaries into circles conformally. After getting all the updated boundary conditions, we obtain the global parameterization of the multiply connected surface by solving the Laplace equation for each subdomain. Using this divide-and-conquer approach, the global conformal and quasi-conformal parameterizations of surfaces can be efficiently computed. Experimental results are presented to demonstrate the effectiveness of our proposed algorithm. More broadly, the proposed shift in perspective from solving a global quasi-conformal mapping problem to solving multiple local mapping problems paves a new way for computational quasi-conformal geometry.

Key words. conformal parameterization, quasi-conformal parameterization, partial welding, multiply connected surface, Koebe's iteration

MSC codes. 65D18, 68U05, 52C26, 30C20

DOI. 10.1137/21M1466323

1. Introduction. In modern applied mathematics and computer science, three-dimensional (3D) surfaces play an important role in many areas, such as brain mapping in medical imaging, 3D model reconstruction in computer graphics, and 3D object detection and classification in computer vision. One important technique for processing 3D models is surface parameterization, which refers to the process of mapping a 3D surface to a two-dimensional (2D) domain based on certain criteria. With the aid of surface parameterization, one can work on

^{*}Received by the editors December 20, 2021; accepted for publication (in revised form) May 20, 2022; published electronically October 27, 2022.

https://doi.org/10.1137/21M1466323

Funding: The work of the second author was partially supported by National Science Foundation grant DMS-2002103. The work of the third author was partially supported by HKRGC GRF project 14306721.

[†]Department of Mathematics, The Chinese University of Hong Kong, Hong Kong (zpzhu@math.cuhk.edu.hk, lmlui@math.cuhk.edu.hk).

[‡]Department of Mathematics, Massachusetts Institute of Technology, Cambridge, MA 02139 USA (ptchoi@mit.edu).

the 2D domain instead of the original 3D surface. For example, to solve a partial differential equation (PDE) on a complicated 3D domain, one can map the domain to a 2D parameter domain and then solve the PDE on it instead. Moreover, with the advancement of 3D scanning and rendering technologies, 3D surfaces with superlarge size and high resolution can be easily obtained nowadays. Therefore, a need arises for fast and accurate algorithms in the parameterization of large meshes.

Among all the surface parameterization methods, conformal parameterizations make up a very special class. Conformality preserves the angular structure at the infinitesimal level and thus preserves the local geometry. This property is advantageous in many tasks that rely on the preservation of local geometry, such as 3D surface remeshing and image registration. Quasi-conformal (QC) maps are a generalization of conformal maps associated with a complex-valued function defined at each point of the source domain called the Beltrami coefficient. Unlike conformal maps, quasi-conformal maps do not preserve local geometry in general. In particular, the Beltrami coefficient defined at each point of the source domain determines the angular distortion at the infinitesimal level at each point. Also, the bijectivity of quasi-conformal maps can be ensured by enforcing the sup-norm of the Beltrami coefficient to be strictly less than 1. Since conformality is a very strict condition that cannot be ensured in many situations with the presence of other constraints, quasi-conformal maps are often utilized. For instance, in image and surface registration, quasi-conformal maps can be used for achieving a balance between the local geometric distortion and the mismatch in prescribed landmark or intensity information of the registered images and surfaces. In recent years, various algorithms have been proposed for computing conformal and quasi-conformal maps. However, most of them are not designed for large meshes, especially those with more complicated topology such as multiply connected meshes.

In this paper, we propose a novel parallelizable method for the computation of quasiconformal parameterization of multiply connected surfaces onto a 2D circular domain, which refers to a connected domain whose complements are several circular disks. As a special case of quasi-conformal maps, conformal maps can also be efficiently computed by our method. Figure 1 gives an overview of our proposed method. Given a multiply connected open surface \mathcal{S} and a prescribed Beltrami coefficient μ , we first partition \mathcal{S} into several smaller subdomains. Then, we compute the free-boundary conformal maps from them to \mathbb{C} in parallel. We then compose a free-boundary quasi-conformal map with the given Beltrami coefficient for each subdomain in parallel. As computing quasi-conformal maps on several small subdomains in a parallel way is much more efficient than computing the global quasi-conformal map directly, our algorithm is more efficient than many existing global parameterization methods. After computing the initial maps, we utilize an idea called partial welding [11] to glue the boundaries of the flattened subdomains along their common arcs. In particular, since \mathcal{S} is a multiply connected surface, we propose a variant of the original partial welding algorithm in [11] to achieve this task. Moreover, in order to transform the boundaries into circles, we propose a parallel version of the Koebe's iteration [39] that is highly compatible with our algorithm. By the composition formula of Beltrami coefficients in quasi-conformal theory [26], the partial welding procedure and the Koebe's iteration will not induce any change in the prescribed Beltrami coefficient μ , as every function involved in these steps is conformal. The computation of partial welding and the parallel Koebe's iteration relies on a method called

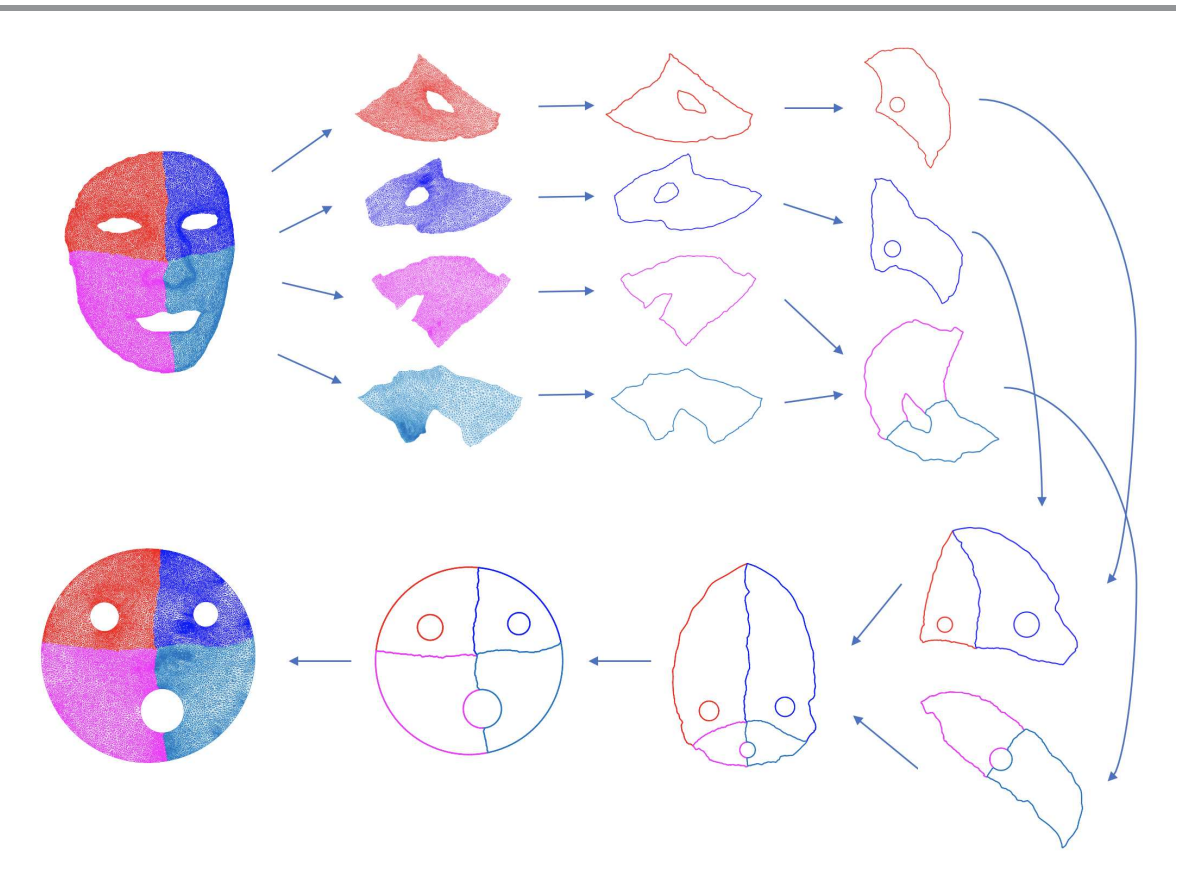


Figure 1. An illustration of our proposed method for the global quasi-conformal parameterization of multiply connected surfaces. Given a multiply connected surface partitioned into several subdomains, we first compute the free-boundary quasi-conformal parameterization for each of them in parallel. Then, we apply our proposed variants of the partial welding method [11] and the Koebe's iteration [39] to find a global conformal mapping of the boundaries of the submeshes to a circular domain with circular holes. Finally, we obtain the global parameterization of the entire surface by solving the Laplace equation on each subdomain in a parallel manner. Note that most of the steps for different subdomains are independent of the other subdomains, and hence the method is highly parallelizable.

the geodesic algorithm [55], whose convergence is theoretically guaranteed under certain mild conditions. All the computations in these two steps only involve the boundary points and welding paths and hence are highly efficient. Finally, using the new boundary conditions generated by the above procedures, we obtain the global quasi-conformal parameterization by solving the Laplace equation on each subdomain in parallel.

The rest of this paper is organized as follows. In section 2, we review the previous works on surface parameterization, with an emphasis on conformal and quasi-conformal parameterizations. In section 3, we introduce the mathematical concepts related to this work. In section 4, we describe our proposed method for the global conformal and quasi-conformal parameterizations of multiply connected surfaces. In section 5, we present experimental results and comparisons with other methods to demonstrate the effectiveness of our method. In section 6, we show several applications of our proposed method in different fields. In section 7, we discuss the limitations of our method and outline possible future research directions.

2. Related works. In the past few decades, surface parameterization has attracted tremendous research attention in the areas of geometry processing, graphics, and computer vision. Detailed surveys and reviews on the topic can be found in [24, 35, 70]. In particular, since in general it is impossible to achieve isometric (both area-preserving and angle-preserving) parameterizations except for surfaces with zero Gaussian curvature, two major types of surface parameterization methods are the area-preserving and the angle-preserving.

Existing area-preserving parameterization methods include the locally authalic map [23], Lie advection [86], optimal mass transport (OMT) [22, 27, 85] (see [2] for a summary of OMT mapping algorithms for both surfaces and volumetric solids), density-equaling map (DEM) [9, 16], and stretch energy minimization (SEM) [78]. Although the area structure of the input surface can be well preserved by these methods, the angle structure is usually significantly distorted. Since the angle structure is closely related to the local geometry of the surface, the distortion in the angle structure may induce obstacles for some applications. In these situations, angle-preserving parameterizations may be preferable.

Existing conformal parameterization methods for simply connected open surfaces include least-squares conformal map (LSCM) [47], discrete natural conformal parameterization (DNCP) [23], angle-based flattening (ABF) [68, 69, 80], holomorphic 1-form [31], discrete Yamabe flow [52, 71], discrete Ricci flow [37, 75, 84], fast disk conformal map [18], boundary first flattening [65], linear disk conformal map [13], conformal energy minimization [77], parallelizable global conformal parameterization (PGCP) [11, 12], and spherical cap conformal map [66]. For simply connected closed surfaces, existing spherical conformal parameterization methods include harmonic energy minimization [30, 43] and its linearizations [3, 10, 17, 32] and the PGCP [11]. While it has been found that many surfaces in real applications are multiply connected, the conformal mapping of multiply connected surfaces has been less studied. Existing conformal mapping methods between multiply connected planar domains include conformal welding [53], Schwarz–Christoffel map [19, 20], slit map [21], and PlgCirMap [57]. For the conformal parameterization of multiply connected surfaces, existing methods include the generalized Koebe's iteration [83], Laurent series [41], discrete conformal equivalence [5], and polyannulus conformal map (PACM) [7].

Quasi-conformal maps are a generalization of conformal maps with bounded local geometric distortion. As they are less restrictive than conformal maps, there has been an increasing interest in quasi-conformal surface parameterization methods in recent years. Existing methods for computing quasi-conformal parameterization include auxiliary metric [82], quasi-Yamabe flow [81], linear Beltrami solver (LBS) [14, 44, 49], Beltrami holomorphic flow (BHF) [51, 58], QC iteration [50, 56], extremal quasi-conformal map [72], bounded distortion map [6, 48], discrete Beltrami flow [73, 74], quasi-conformal energy minimization (QCMC) [34], and least-squares quasi-conformal map (LSQC) [63]. In recent years, quasi-conformal maps have been used in various applications, such as image and surface registrations [44, 64, 79] and shape analysis [8, 15].

3. Mathematical background.

3.1. Quasi-conformal theory. In this subsection, we briefly introduce quasi-conformal maps on the complex plane and on Riemann surfaces. For details, the reader is referred to [4, 26].

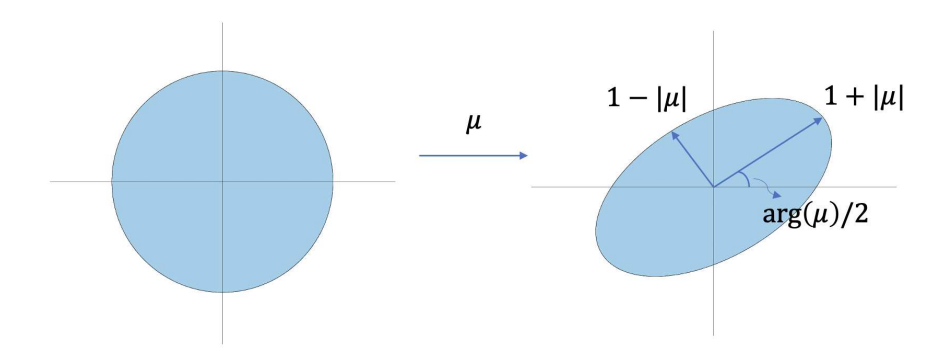


Figure 2. An illustration of how the Beltrami coefficient determines the conformality distortion at the infinitesimal level, i.e., the differential map at a point associated with Beltrami coefficient μ .

Quasi-conformal maps are a generalization of conformal maps and can be understood as maps with bounded conformality distortion. An orientation-preserving homeomorphism $f: \Omega \subset \mathbb{C} \to \Omega' \subset \mathbb{C}$ is said to be a *quasi-conformal map* if it satisfies the Beltrami equation

(3.1)
$$\frac{\partial f}{\partial \bar{z}} = \mu_f(z) \frac{\partial f}{\partial z},$$

where $\mu_f(z)$ is a complex-valued Lebesgue-measurable function satisfying $\|\mu_f(z)\|_{\infty} < 1$ called the *Beltrami coefficient* of f. $\mu_f(z)$ encodes the information about the conformality distortion of f. If $\mu_f(z) = 0$ for all z, then (3.1) becomes the Cauchy–Riemann equation, and hence f is conformal. Geometrically, a quasi-conformal mapping maps infinitesimal circles to infinitesimal ellipses with eccentricity determined by the Beltrami coefficient (see Figure 2).

The following theorem by Ahlfors and Bers, called the *measurable Riemann mapping theorem* [1], is a generalization of the Riemann mapping theorem for conformal maps to the case of quasi-conformal maps.

Theorem 3.1 (measurable Riemann mapping theorem). Suppose $\mu: \mathbb{C} \to \mathbb{C}$ is Lebesgue measurable and satisfies $\|\mu\|_{\infty} < 1$. Then there is a quasi-conformal homeomorphism ϕ from \mathbb{C} onto itself, which is in the Sobolev space $W^{1,2}(\mathbb{C})$ and satisfies the Beltrami equation (3.1) in the distribution sense. Furthermore, by fixing 0, 1, and ∞ , the associated quasi-conformal homeomorphism ϕ is uniquely determined.

Conversely, given an orientation-preserving homeomorphism ϕ , we can compute its Beltrami coefficient μ_{ϕ} using the Beltrami equation (3.1) as follows:

(3.2)
$$\mu_{\phi}(z) = \frac{\partial \phi}{\partial \bar{z}} / \frac{\partial \phi}{\partial z}.$$

This gives the following relation between the Jacobian J_{ϕ} and the Beltrami coefficient μ_{ϕ} :

(3.3)
$$J_{\phi}(z) = \left| \frac{\partial \phi}{\partial z} \right|^2 \left(1 - |\mu_{\phi}(z)| \right)^2.$$

Note that $J_{\phi}(z) > 0$ everywhere as ϕ is an orientation-preserving homeomorphism, and hence we must have $|\mu_{\phi}(z)| < 1$ for all z. By the measurable Riemann mapping theorem and the above observation, we conclude that there is a one-to-one correspondence between normalized quasi-conformal homeomorphisms and Beltrami coefficients strictly less than 1.

Moreover, we have the following composition formula for the Beltrami coefficient of a composition of two quasi-conformal maps. Suppose $f, g : \mathbb{C} \to \mathbb{C}$ are quasi-conformal maps with Beltrami coefficients μ_f and μ_g , respectively. Then, the Beltrami coefficient of $g \circ f$ is

(3.4)
$$\mu_{g \circ f} = \frac{\mu_f + (\mu_g \circ f)\tau}{1 + \bar{\mu}_f(\mu_g \circ f)\tau}, \quad \tau = \frac{\bar{f}_z}{f_z}.$$

In particular, if g is a conformal map, we have $\mu_{g \circ f} = \mu_f$. In other words, given a quasiconformal map f with Beltrami coefficient μ , the Beltrami coefficient of $g \circ f$ is always μ for any conformal map g. This observation plays an important role in our proposed algorithm for multiply connected quasi-conformal parameterization.

The following theorem relates the regularity of a quasi-conformal map with its Beltrami coefficient [4].

Theorem 3.2. Suppose $f \in W^{1,2}_{loc}(\mathbb{C},\mathbb{C})$ is the solution to the Beltrami equation (3.1), where the Beltrami coefficient $\mu(z) \in C^{l,\alpha}_{loc}(\mathbb{C},\mathbb{C}), \|\mu\|_{\infty} < 1$. Then, $f \in C^{l+1,\alpha}_{loc}(\mathbb{C},\mathbb{C})$.

For quasi-conformal maps of Riemann surfaces, one can generalize the concept of Beltrami coefficients to Beltrami differentials via the local charts of the surfaces. More specifically, the Beltrami differential $\mu(z)\frac{d\bar{z}}{dz}$ on a Riemann surface S is an assignment to each chart $(U_{\alpha}, \phi_{\alpha})$ of an L_{∞} complex-valued function μ_{α} , defined on local parameters z_{α} , such that

(3.5)
$$\mu_{\alpha}(z_{\alpha})\frac{d\bar{z}_{\alpha}}{dz_{\alpha}} = \mu_{\beta}(z_{\beta})\frac{d\bar{z}_{\beta}}{dz_{\beta}}$$

on the domain which is also covered by another chart $(U_{\beta}, \phi_{\beta})$, where $\frac{dz_{\beta}}{dz_{\alpha}} = \frac{d}{dz_{\alpha}}\phi_{\alpha\beta}$ and $\phi_{\alpha\beta} = \phi_{\beta} \circ \phi_{\alpha}^{-1}$. In particular, if a surface can be covered by a single chart, we can use the Beltrami coefficient defined on that chart to represent the Beltrami differential of the surface. As our work focuses on multiply connected open surfaces, we can simply find a free-boundary conformal map from the given surface onto $\mathbb C$ and use that as the global chart to represent the Beltrami differential. Therefore, the Beltrami coefficient and the Beltrami differential are used interchangeably in our method.

3.2. Variational formulation of quasi-conformal map. Here we introduce a variational approach called the least-squares quasi-conformal map (LSQC), developed by Qiu, Lam and Lui [63], for solving the Beltrami equation (3.1) to get free-boundary quasi-conformal maps. The formulation is an analogue of the DNCP/LSCM formulation [23, 47] for free-boundary conformal maps of 2D domains. Suppose $f: \Omega \subset \mathbb{C} \to \Omega' \subset \mathbb{C}$ is a quasi-conformal map. We write f = u + iv and $\mu_f = \rho + i\tau$, where u, v, ρ , and τ are real-valued functions. Also, let

(3.6)
$$A = \frac{1}{1 - |\mu|^2} \begin{pmatrix} (\rho - 1)^2 + \tau^2 & -2\tau \\ -2\tau & (1 + \rho)^2 + \tau^2 \end{pmatrix}.$$

From the above, we can transform the Beltrami equation (3.1) into

(3.7)
$$\begin{pmatrix} u_x \\ u_y \end{pmatrix} = \begin{pmatrix} 0 & 1 \\ -1 & 0 \end{pmatrix} A \begin{pmatrix} v_x \\ v_y \end{pmatrix}.$$

Then, using the relation $u_{xy} = u_{yx}$, we obtain the equation

(3.8)
$$\nabla \cdot (A\nabla v(z)) = 0.$$

Similarly, we can express v_x, v_y in terms of u_x, u_y and get

$$(3.9) \nabla \cdot (A\nabla u(z)) = 0.$$

It can be observed that the two equations above are the Euler-Lagrange equations of the following two Dirichlet-type energies, respectively:

(3.10)
$$E_A(u) = \frac{1}{2} \int_{\Omega} \left\| A^{1/2} \nabla u \right\|^2 dx dy, \quad E_A(v) = \frac{1}{2} \int_{\Omega} \left\| A^{1/2} \nabla v \right\|^2 dx dy.$$

Note that (3.8) and (3.9) are necessary conditions of u and v derived from the Beltrami equation (3.1). One can also define the following least-squares quasi-conformal energy using the Beltrami equation (3.1) directly:

(3.11)
$$E_{QC}^{\mu}(u,v) = \frac{1}{2} \int_{\Omega} \|P\nabla u + JP\nabla v\|^2 dx dy,$$

where

(3.12)
$$P = \frac{1}{\sqrt{1-|\mu|^2}} \begin{pmatrix} 1-\rho & -\tau \\ -\tau & 1+\rho \end{pmatrix} \quad \text{and} \quad J = \begin{pmatrix} 0 & -1 \\ 1 & 0 \end{pmatrix}.$$

Since $P^TP = A$, the Beltrami equation (3.1) holds if and only if $E_{QC}^{\mu}(u, v) = 0$. The following equation relates the three energies $E_A(u)$, $E_A(v)$, and $E_{QC}^{\mu}(u, v)$:

(3.13)
$$E_A(u) + E_A(v) - E_{QC}^{\mu}(u, v) = \mathcal{A}(u, v) = \int_{\Omega} (u_x v_y - v_x u_y) dx dy.$$

Since f is an orientation-preserving homeomorphism, $\mathcal{A}(u,v)$ is the area of $\Omega' = f(\Omega)$. For this reason, $\mathcal{A}(u,v)$ is called the *area functional*. Now, since $E_{QC}^{\mu}(u,v)$ is always positive, we have the following inequality:

$$(3.14) E_A(u) + E_A(v) \ge \mathcal{A}(u, v).$$

The equality holds if and only if $E_{QC}^{\mu}(u,v)=0$, i.e., the Beltrami coefficient of f=u+iv is equal to μ .

Later on, we will see that $E_A(u)$, $E_A(v)$, and A(u,v) can all be efficiently computed numerically, which allows us to compute free-boundary quasi-conformal maps efficiently.

On the other hand, if we want to compute a map from a domain to some specific domain such as a disk or a rectangle, we need to specify the boundary conditions. Suppose we want to compute a quasi-conformal map f from a simply connected domain Ω to the unit disk \mathbb{D} . By the measurable Riemann mapping theorem, f is unique up to a Möbius transformation. Therefore, the boundary condition $f(\partial\Omega)$ should be carefully set; otherwise, such a quasi-conformal map may not exist. To get the admissible boundary condition, we are going to use the geodesic algorithm developed by Marshall and Rohde [55], which will be introduced later in this paper. By the elliptic PDE theory, with the admissible boundary condition, (3.8) and (3.9) have a unique solution and yield the desired quasi-conformal map.

Finally, we remark that since conformal maps are a special case of quasi-conformal maps with $\mu \equiv 0$, the above results also hold for conformal maps and are consistent with the results in the conformal mapping literature [36, 62].

3.3. Conformal welding. There are several equivalent ways to describe the conformal welding problem. Here, we adopt the version in [53, 67]. Let $\bar{\mathbb{C}} := \mathbb{C} \cup \{\infty\}$ denote the extended complex plane and \mathbb{D} denote the unit disk $\{z \in \mathbb{C} : |z| \leq 1\}$. Given an increasing homeomorphism h of $\partial \mathbb{D}$, the conformal welding problem is to find a Jordan curve J and two conformal maps f, g such that f and g map \mathbb{D} and $\bar{\mathbb{C}}\setminus \mathrm{int}(\mathbb{D})$ to $J \cup \mathrm{int}(J)$ and $J \cup \mathrm{ext}(J)$, respectively, where $\mathrm{int}(J)$ and $\mathrm{ext}(J)$ are the interior and exterior of J, respectively, and f(h(x)) = g(x) on $\partial \mathbb{D}$. Since there exists a conformal map between the unit disk and the upper half plane, we can also formulate the problem for the upper and lower half planes with an increasing homeomorphism on the real axis.

The conformal welding problem may not have a solution for a general homeomorphism h. However, the existence of conformal welding can be proved if h satisfies certain conditions. Here, we introduce the notion of quasi-symmetric functions. Let h be a continuous, strictly increasing function defined on an interval I of the x-axis. We call h k-quasi-symmetric on I [46] if there exists a positive constant k such that

(3.15)
$$\frac{1}{k} \le \frac{h(x+t) - h(x)}{h(x) - h(x-t)} \le k$$

for all $x, x - t \in I$ with t > 0.

The following theorem shows the solvability of the conformal welding problem when h is a quasi-symmetric homeomorphism of the real axis.

Theorem 3.3 (sewing theorem [46]). Let h be a quasi-symmetric function on the real axis. Then the upper and lower half planes can be mapped conformally onto disjoint Jordan domains D, Ω by two maps ϕ, ϕ^* , such that $\phi(x) = \phi^*(h(x))$ for all $x \in \mathbb{R}$.

The proof of the above theorem is based on approximation techniques of quasi-symmetric functions. The solvability of the conformal welding problem can also be proved using the existence of solutions to the Beltrami equation as shown by Pfluger [61].

3.4. Geodesic algorithm. The Riemann mapping theorem guarantees the existence of a conformal map from a simply connected open subset of \mathbb{C} to the unit disk, unique up to a Möbius transformation. However, this theorem does not provide a way to compute such a conformal map explicitly. In the 1980s, Kühnau [42] and Marshall and Morrow [54]

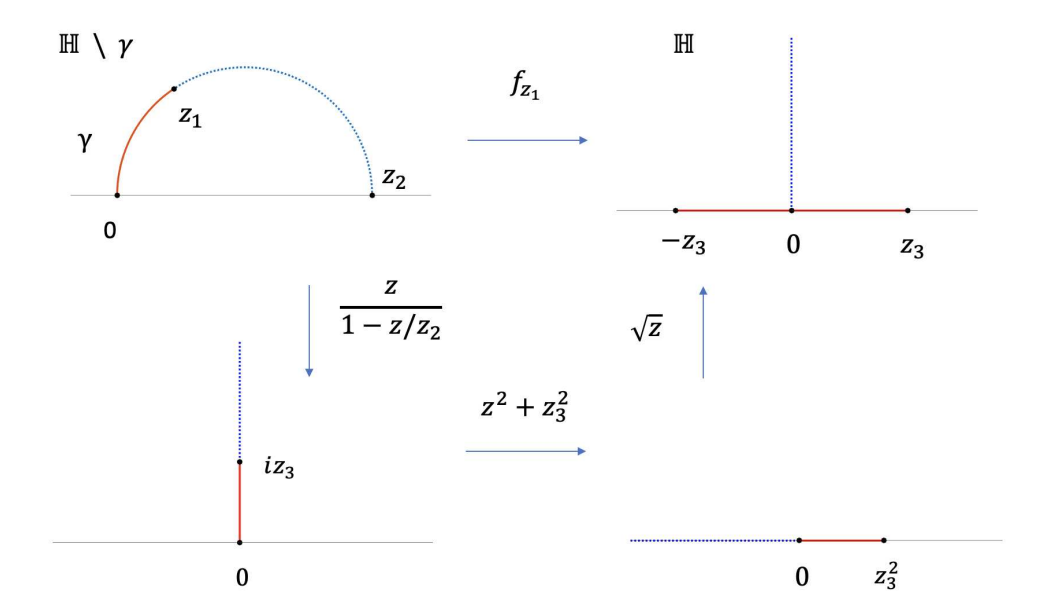


Figure 3. The basic conformal map f_{z_1} of the geodesic algorithm in [55].

independently proposed the *zipper algorithm* for computing conformal maps from a simply connected open set to the unit disk. Later, Marshall and Rohde [55] proved the convergence in different cases for a variant of the zipper algorithm called *geodesic algorithm*. As described by Marshall and Rohde [55], the geodesic algorithm can be viewed as an approximate solution to a conformal welding problem or as a discretization of the Loewner differential equation. The details, variants, and convergence of the geodesic algorithm can be found in [55]. Below, we briefly introduce the geodesic algorithm.

The key ingredient of the geodesic algorithm is the twofold map shown in Figure 3, which is a composition of a Möbius transformation, a square map, and a square root map. In one direction, it maps a hyperbolic geodesic to the real axis. Given z_1 on the upper half plane, we denote by the red line γ the circular arc from 0 to z_1 , which is a hyperbolic geodesic. The map f_{z_1} conformally maps γ to $[0, z_3]$ or $[-z_3, 0]$ depending on the choice of the branch for the square root map. The rest of the upper half plane $\mathbb{H}\backslash\gamma$ is conformally mapped to \mathbb{H} . In the reverse direction, note that two line segments $[-z_3, 0]$ and $[0, z_3]$ are both mapped to $[0, z_3^2]$ by a square map and eventually mapped to the curve γ . Hence, this direction allows us to conformally align two different lines, which can then be used to compute conformal welding.

In order to compute a Riemann mapping from some Jordan domain Ω to \mathbb{H} by the geodesic algorithm, we only need a sequence of boundary points $\{z_0, z_1, \ldots, z_n\}$ of $\partial\Omega$ that are sufficiently dense on $\partial\Omega$. The starting map is given by

(3.16)
$$g_1(z) = i\sqrt{\frac{z - z_1}{z - z_0}},$$

with $g_1(z_1)=0$ and $g_1(z_0)=\infty$. Let $\xi_2=g_1(z_2)$ and $g_2=f_{\xi_2}$, where f_{ξ_2} is the map defined

in Figure 3. We repeat this process for all the boundary points to get

and

$$(3.18) g_k = f_{\mathcal{E}_k}$$

for k = 2, ..., n. We then compute a final map by defining

and

(3.20)
$$g_{n+1} = \pm \left(\frac{z}{1 - z/\xi_{n+1}}\right)^2,$$

where the positive sign is chosen when the data points are in counterclockwise orientation, and the negative sign is chosen otherwise. The composition mapping $g = g_{n+1} \circ g_n \circ \cdots \circ g_1$ gives a conformal map from Ω to \mathbb{H} . Although originally invented to be in this form, as indicated by Marshall and Rohde in [55], the computation of the mapping is more reliable when we perform it on the right half plane instead of the upper half plane due to the default choice of branching in scientific computing software. In our algorithm, we perform all the computation on the right half plane.

The convergence of the geodesic algorithm was proved in [55]. In particular, under different assumptions on the regularity of the region Ω , different convergence results can be established.

3.5. Riemann mapping theorem for multiply connected domains. While the Riemann mapping theorem focuses on the conformal equivalence between any simply connected region in the complex plane and the open unit disk, there is also a generalization of this result to multiply connected domains. Here, we present a result given in Chapter 17 of [33], which shows that any region R of connectivity $n \ge 2$ can be conformally mapped to the complement of n closed circular disks. Such a region is called a circular region of connectivity n.

Theorem 3.4. Let R be a region of connectivity $n \geq 2$ in the extended complex plane with $\infty \in R$. Then, there exists a unique circular region C of connectivity n and a unique one-to-one analytic function f satisfying $f(z) = z + O(\frac{1}{z})$ such that f(R) = C.

The book [33] gives a constructive proof of this theorem, which was originally due to Koebe and hence called the *Koebe's iteration* [39]. We explain the Koebe's iteration in detail here, as it is closely related to our proposed algorithm in this paper. Suppose the components of complements of R are K_1, K_2, \ldots, K_n . Let $R_0 := R, D_{0,i} := K_i, i = 1, 2, \ldots, n$. Suppose in the (k-1)th iteration we have obtained a region R_{k-1} of connectivity n, whose complements are $D_{k-1,i}, i = 1, 2, \ldots, n$. Then, in the kth iteration, let $j = k \mod n, 1 \le j \le n$. We find the unique conformal map h_k , normalized at ∞ , from $R_{k-1} \setminus D_{k-1,j}$ to the exterior of a disk. Let $D_{k,j}$ be that disk, and let

$$(3.21) R_k := h_k(R_{k-1}), \ D_{k,i} := h_k(D_{k,i-1}), \ i = 1, 2, \dots, n, \ i \neq j.$$

Clearly, R_k is a region of connectivity n, and the components of complements of it are $D_{k,i}$, i = 1, 2, ..., n. The Koebe's algorithm progresses cyclically on i = 1, 2, ..., n, each time mapping one boundary component to a circle until the result converges.

Let f denote the desired Riemann mapping, $f_k := h_k \circ h_{k-1} \circ \cdots \circ h_1$ and $g_k := f_k \circ f^{-1}$. We have the following estimate of the convergence rate [33].

Theorem 3.5. There exist constants $\gamma > 0$ and $0 < \mu < 1$ such that for $k = 1, 2, \ldots$ and for all $w \in C$,

$$(3.22) |g_k(w) - w| \le \gamma \mu^{4[k/n]}$$

Numerically, in each iteration we apply the geodesic algorithm to transform one of the boundaries into a circle and also update the coordinates of other boundaries [53]. In practice, we find that the algorithm exhibits fast convergence, and usually we can already obtain a satisfactory result after performing only one iteration for each boundary. One example can be found in Figure 4. As we shall see later, that is part of the reason why our proposed parallel Koebe's iteration method works. We remark that Zeng et al. [83] proposed a generalized Koebe's iteration method that handles two boundaries at each iteration and proved that it converges quadratically faster than the conventional Koebe's algorithm. In our proposed method, for simplicity we adopt the conventional Koebe's algorithm to exploit parallelism. Nevertheless, it may be possible to develop a similar parallelizable algorithm using the generalized Koebe's iteration method.

Below, we also state the extension of the Riemann mapping theorem for multiply connected domains to quasi-conformal maps presented in the book [45].

Theorem 3.6. Let D be the closure of a domain bounded by n disjoint Jordan curves. Suppose μ is a measurable function defined in D and $\|\mu\|_{\infty} < 1$. Then, there exist a closed canonical circular domain D' of connectivity n and a solution f to the Beltrami equation (3.1), which represents a quasi-conformal homeomorphism of D onto D', determined uniquely up to conformal maps of D' onto itself.

In practice, given a multiply connected domain D with a prescribed Beltrami coefficient μ , we can first compute a free-boundary quasi-conformal parameterization of it onto a domain D_1 . After that, we compute the conformal map from D_1 to a circular domain D_2 using the Koebe's iteration. The composition of these two maps gives the desired result.

4. Proposed method.

4.1. An overview of our proposed method. Let \mathcal{S} be a multiply connected surface in \mathbb{R}^3 represented by a triangle mesh $(\mathcal{V}, \mathcal{F})$, where \mathcal{V} denotes the set of vertices and \mathcal{F} denotes the set of faces. Given a target Beltrami coefficient μ , we aim to efficiently and accurately compute the global quasi-conformal parameterization of \mathcal{S} onto the unit disk with circular holes.

First, we partition the entire mesh S into multiple submeshes S_i , i = 1, ..., m, such that each submesh is either simply connected or multiply connected with one inner hole of S. Note that we may further partition the submeshes with one hole into smaller simply connected submeshes if necessary. Then, we compute a free-boundary conformal parameterization

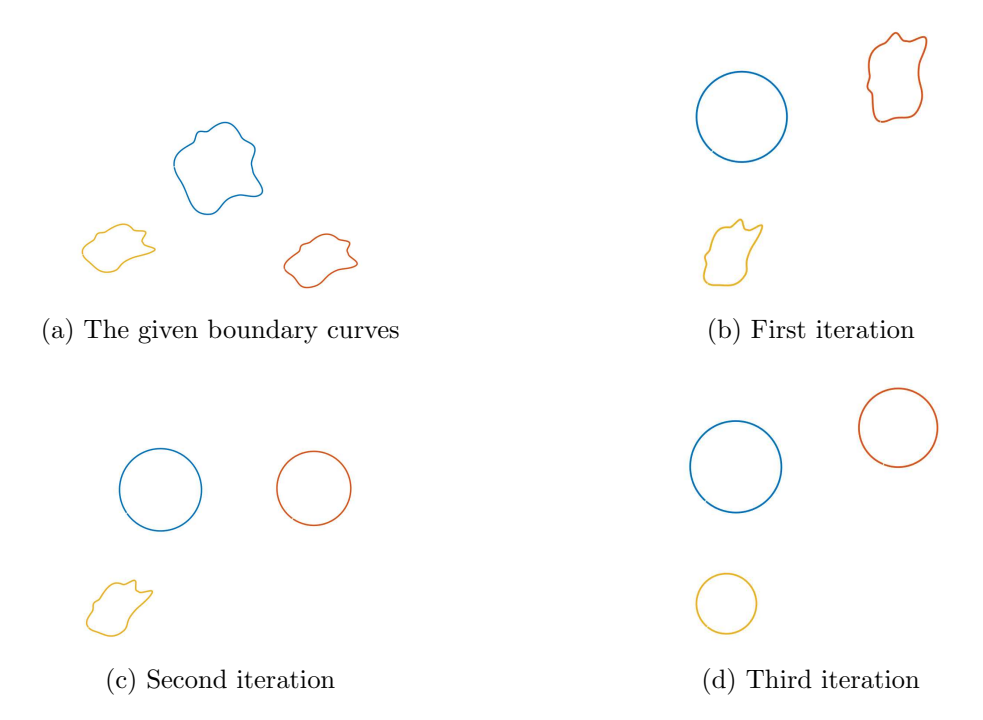


Figure 4. An example illustrating the fast convergence of the Koebe's iteration method, with each map computed using the geodesic algorithm.

 $\varphi_i^c: \mathcal{S}_i \to \mathbb{C}$ of each submesh onto the plane, respectively. Here, we compute the conformal parameterization first because the Beltrami differentials on the surface depend on the choice of isothermal local charts, and the computed free-boundary conformal parameterization serves well in this role for the submeshes. The next step is to compute a free-boundary quasiconformal map of each flattened submesh $\varphi_i^{qc}:\varphi_i^c(\mathcal{S}_i)\to\mathbb{C}$ based on the prescribed Beltrami coefficient, so that the composition $\varphi_i = \varphi_i^{qc} \circ \varphi_i^c$ gives the free-boundary quasi-conformal parameterization for every submesh. Note that both the conformal parameterization and quasi-conformal mapping steps are highly parallelizable, as the computations for different submeshes are independent. Since all the remaining steps only involve conformal transformations, by the composition formula (3.4), the Beltrami coefficient will be preserved by the remaining steps. We apply the geodesic algorithm to transform all the inner holes of the submeshes into circles. This step can be understood as a parallelizable version of the Koebe's iteration. We then apply the welding algorithm to obtain the desired boundary conditions of all submeshes. Note that the inner boundaries after welding are highly circular, as will be illustrated both theoretically and experimentally in the following sections. Finally, we solve the Laplace equation with the updated boundary conditions to obtain the quasi-conformal parameterization for each submesh; together, all the submeshes seamlessly form the desired global quasi-conformal parameterization (see Figure 1 for an illustration).

4.2. Surface partition. We first partition the given multiply connected surface S into multiple submeshes S_i , i = 1, ..., m, which can be done by existing mesh partitioning algorithms or by manually prescribing some edges as the partition cuts. Suppose S contains

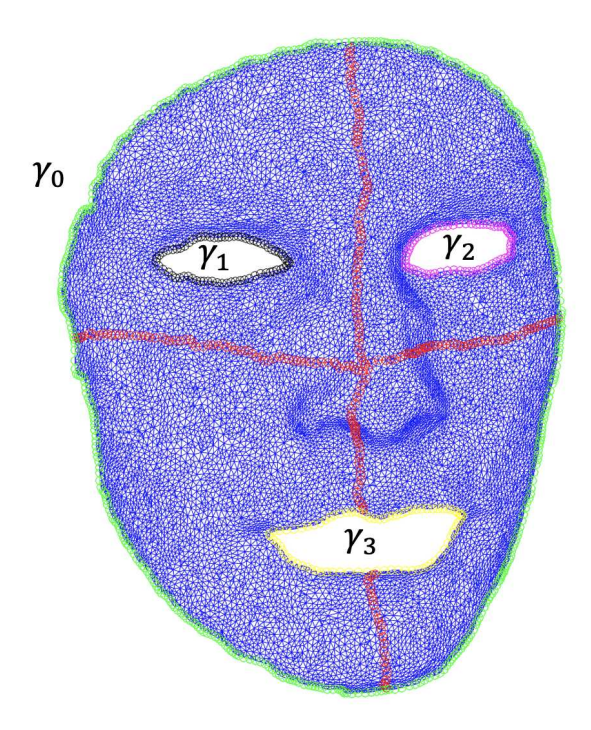


Figure 5. An illustration of the surface partition step. Suppose the surface S contains an outer boundary γ_0 and k disjoint inner boundaries $\{\gamma_i\}_{i=1}^k$ (k=3 in this example). \mathcal{E}_{cut} is a set of chosen prescribed cutting edges (highlighted in red) that does not contain any boundary edges. S can then be partitioned into m submeshes S_1, \ldots, S_m (m=4 in this example) so that each S_i is either simply connected or multiply connected with one inner hole.

an outer boundary γ_0 and k disjoint inner boundaries $\{\gamma_i\}_{i=1}^k$, where each γ_i is represented by a set of boundary edges. The partition procedure consists of the following two steps. In the first step, we choose a set of cutting edges denoted by \mathcal{E}_{cut} such that \mathcal{E}_{cut} does not contain any boundary edges. The reason is that if we remove $\mathcal{E}_{cut} \cup \gamma_0$ from \mathcal{S} , we may obtain several subdomains that are disconnected from one another. Hence, we choose the partition $\mathcal{S} = \bigcup_{i=1}^m \mathcal{S}_i$ by assigning \mathcal{S}_i to be each of the components. In other words, we obtain $\mathcal{S}_1 = (\mathcal{V}_1, \mathcal{F}_1), \mathcal{S}_2 = (\mathcal{V}_2, \mathcal{F}_2), \ldots, \mathcal{S}_m = (\mathcal{V}_m, \mathcal{F}_m)$ (see Figure 5 for an illustration). Mathematically, the following conditions should be satisfied:

(4.1)
$$\mathcal{E}_{cut} \cap \gamma_i = \emptyset \text{ for all } i = 1, \dots, k,$$

and

(4.2)
$$S_i \cap S_j \subset \mathcal{E}_{cut} \text{ or } S_i \cap S_j = \emptyset \text{ for all } i, j = 1, \dots, m.$$

Here, we restrict all S_i to be simply connected or multiply connected with only one inner hole. Such a restriction reduces the difficulty of computing partial welding for multiply connected meshes and performing the parallel Koebe's iteration, as will be explained later. In the second step, we can further partition the submeshes into smaller meshes if necessary. For

example, if a submesh S_i with one hole is still a large mesh, we can partition it into several simply connected meshes.

4.3. Free-boundary quasi-conformal parameterization of the submeshes. After getting the submeshes S_i , i = 1, ..., m, we compute a free-boundary conformal parameterization of each of them onto the plane followed by a free-boundary quasi-conformal map using the variational formulation in section 3.2 by a finite element approach.

The numerical computation of the quasi-conformal mapping follows the implementation described in [63]. Given a flattened triangle mesh Ω represented by a set of vertices $\{w_1, w_2, \ldots, w_n\}$ and a set of triangle faces, we discretize the prescribed Beltrami coefficient μ on Ω by assuming that μ is piecewise constant on each triangle face, i.e., $\mu = \mu_T$ for some constant μ_T on each triangle face T of Ω . We aim to compute a map $f = u + iv : \Omega \to \tilde{\Omega}$, where $\tilde{\Omega}$ is a triangle mesh with the same connectivity as Ω such that f satisfies the Beltrami equation (3.1) in the sense that f is piecewise linear on each face T and $\mu_f|_T = \mu_T$ for each face T. We denote the vertices of $\tilde{\Omega}$ by $\{f(w_1), f(w_2), \ldots, f(w_n)\} = \{u_1 + iv_1, u_2 + iv_2, \ldots, u_n + iv_n\}$. Let $u = \begin{pmatrix} u_1 & u_2 & \cdots & u_n \end{pmatrix}^T$ and $v = \begin{pmatrix} v_1 & v_2 & \cdots & v_n \end{pmatrix}^T$.

We then discretize the energies $E_A(u) = \int_{\Omega} ||A^{1/2} \nabla u||^2$ and $E_A(v) = \int_{\Omega} ||A^{1/2} \nabla v||^2$ in (3.10) in the following way. Let T be an arbitrary triangle with vertices $[w_0^T, w_1^T, w_2^T]$. Suppose the image of T under f is $[f(w_0^T), f(w_1^T), f(w_2^T)] = [u_0^T + iv_0^T, u_1^T + iv_1^T, u_2^T + iv_2^T]$. Since f is linear on T, we can express the gradient of f as

(4.3)
$$\nabla u|_{T} = \frac{1}{2\operatorname{Area}(T)} \begin{pmatrix} 0 & -1 \\ 1 & 0 \end{pmatrix} \sum_{i=0}^{2} u_{i} (w_{2+i}^{T} - w_{1+i}^{T})$$

and

(4.4)
$$\nabla v|_{T} = \frac{1}{2\operatorname{Area}(T)} \begin{pmatrix} 0 & -1 \\ 1 & 0 \end{pmatrix} \sum_{i=0}^{2} v_{i} (w_{2+i}^{T} - w_{1+i}^{T}).$$

Since μ is piecewise constant on each face T, the matrix A given by (3.6) is a constant matrix determined by μ_T on each T. We can then discretize $\int_{\Omega} \left\| A^{1/2} \nabla u \right\|^2$ and $\int_{\Omega} \left\| A^{1/2} \nabla v \right\|^2$ by summing over all faces. We then obtain two quadratic forms

(4.5)
$$E_A(u) = u^T \mathcal{L}_{\mu} u \quad \text{and} \quad E_A(v) = v^T \mathcal{L}_{\mu} v,$$

where \mathcal{L}_{μ} is a symmetric matrix called the *generalized Laplacian matrix*. Furthermore, using (4.3) and (4.4), we can discretize the area matrix $\mathcal{A}(u,v) = \int_{\Omega} u_x v_y - v_x u_y$ in (3.14) as another quadratic form

(4.6)
$$\mathcal{A}(u,v) = \begin{pmatrix} u^T & v^T \end{pmatrix} \begin{pmatrix} 0 & U \\ -U & 0 \end{pmatrix} \begin{pmatrix} u \\ v \end{pmatrix}$$

for some skew-symmetric matrix U. Let

(4.7)
$$M = \begin{pmatrix} \mathcal{L}_{\mu} & 0 \\ 0 & \mathcal{L}_{\mu} \end{pmatrix} - \begin{pmatrix} 0 & U \\ -U & 0 \end{pmatrix}.$$

Note that M is symmetric. By (3.13), to obtain the desired free-boundary quasi-conformal map, it suffices to solve the equation

(4.8)
$$E_{\mathrm{QC}}^{\mu}(u,v) = \begin{pmatrix} u^T & v^T \end{pmatrix} M \begin{pmatrix} u \\ v \end{pmatrix} = 0.$$

We have the following theorem.

Theorem 4.1. The solution of (4.8) is unique under scaling, rotation, and translation.

Proof. Since M is symmetric, it suffices to solve the equation

$$M\begin{pmatrix} u \\ v \end{pmatrix} = 0.$$

Suppose we fix two arbitrary points from $\{f(w_1), f(w_2), \dots, f(w_n)\}$. Then, we need to solve

$$(4.10) B \begin{pmatrix} u \\ v \end{pmatrix} = b$$

for some matrix B and vector b. A direct consequence of Proposition 2.13 in [63] is that the matrix B is of full rank. Hence, we obtain a unique solution if two arbitrary points are fixed.

On the other hand, suppose $\binom{u_0}{v_0}$ is one solution to (4.8). Then, it is easy to check that for any $k \in \mathbb{R}$, we have

$$(4.11) M\begin{pmatrix} ku_0 \\ kv_0 \end{pmatrix} = 0.$$

Also, for any $\theta \in [0, 2\pi]$, let $u_1 = \cos \theta u_0 - \sin \theta v_0$ and $v_1 = \sin \theta u_0 + \cos \theta v_0$. We have

$$(4.12) M \begin{pmatrix} u_1 \\ v_1 \end{pmatrix} = 0.$$

Further, notice that if we let $f(w_i) = (x_0, y_0)$ for some x_0, y_0 for all i = 1, ..., n, then clearly $E_A(u)$, $E_A(v)$, and A(u, v) are all zero. As a result, for any $x, y \in \mathbb{R}$,

$$M\begin{pmatrix} u_0 + x \\ v_0 + y \end{pmatrix} = 0.$$

Suppose the unique solution we obtain by fixing $f(w_i)$ and $f(w_j)$ to (x_i, y_i) and (x_j, y_j) , respectively, is $\binom{u_0}{v_0}$. We can transform $\binom{u_0}{v_0}$ by scaling, rotation, and translation so that $f(w_s) = (x_s, y_s)$ and $f(w_t) = (x_t, y_t)$ for arbitrary $s, t, (x_s, y_s), (x_t, y_t)$. We denote the transformed data points by $\binom{u_0}{v_0}$. Notice that this is exactly the unique solution we can obtain by fixing $f(w_s)$ and $f(w_t)$ to (x_s, y_s) and (x_t, y_t) , respectively. This completes the proof.

As for the boundary conditions for solving the linear system, we usually set the target positions of two boundary vertices that are far away from each other in \mathcal{M} as (0,0) and (1,0) to control the scale of the free-boundary mapping result.

Since the Beltrami differential on a surface in \mathbb{R}^3 depends on the choice of local chart (see section 3.1), we cannot directly apply this method to compute a quasi-conformal flattening of a surface. Instead, we need to first compute a free-boundary conformal flattening φ^c of a surface \mathcal{S} onto \mathbb{C} and then apply the above method to get a free-boundary quasi-conformal map φ^{qc} in \mathbb{C} . For the conformal flattening map $\varphi^c = (u, v) : \mathcal{S} \to \tilde{\Omega}$, the Dirichlet energy can be discretized as

$$(4.14) E(u) + E(v) = \frac{1}{2} \int_{\mathcal{S}} (\|\nabla u\|^2 + \|\nabla v\|^2) = \begin{pmatrix} u^T & v^T \end{pmatrix} \begin{pmatrix} \mathcal{L} & 0 \\ 0 & \mathcal{L} \end{pmatrix} \begin{pmatrix} u \\ v \end{pmatrix},$$

where \mathcal{L} is the cotangent Laplacian matrix [62]. The DNCP method [23] discretizes the area using an approach different from (4.6). Specifically, by Green's theorem,

(4.15)
$$\mathcal{A}(\varphi^c) = \int_{\tilde{\Omega}} dx \, dy = \frac{1}{2} \oint_{\partial \tilde{\Omega}} -y \, dx + x \, dy.$$

Therefore, in the simply connected case which [23] focuses on, the area is discretized as

(4.16)
$$\mathcal{A}(\varphi^c) = \frac{1}{2} \sum_{[w_i, w_i] \in \partial \mathcal{S}} (u_i v_j - u_j v_i) = \begin{pmatrix} u^T & v^T \end{pmatrix} Q \begin{pmatrix} u \\ v \end{pmatrix}$$

for some symmetric matrix Q. The free-boundary conformal parameterization φ^c is then obtained by solving

(4.17)
$$\left(\begin{pmatrix} \mathcal{L} & 0 \\ 0 & \mathcal{L} \end{pmatrix} - Q \right) \begin{pmatrix} u \\ v \end{pmatrix} = 0.$$

In our case, some submeshes obtained from the partition step may be multiply connected. To apply the DNCP formulation for parameterizing them, a natural extension of (4.16) for multiply connected meshes is presented below. Let S be a multiply connected mesh. Denote the outer boundary of it as γ_0 and the inner boundaries as $\gamma_1, \ldots, \gamma_p$, where $p \geq 1$. The area $\mathcal{A}(\varphi^c)$ can then be discretized as

(4.18)
$$\mathcal{A}(\varphi^c) = \mathcal{A}_0 - \mathcal{A}_1 - \dots - \mathcal{A}_p,$$

where A_0, \ldots, A_p are the areas of the regions enclosed by $\gamma_0, \ldots, \gamma_p$, respectively. Each of them can be computed using the formula in (4.16). Since all terms are expressed using the corresponding boundary vertices in S, the area $A(\varphi)$ can again be written in the form $\begin{pmatrix} u^T & v^T \end{pmatrix} \tilde{Q} \begin{pmatrix} u \\ v \end{pmatrix}$ for some matrix \tilde{Q} . We can then replace Q with \tilde{Q} in (4.17) and solve it to obtain the free-boundary conformal parameterization φ^c .

Remark 4.2. Careful checking reveals that the two approaches for discretizing the area functional in (4.6) and (4.18) in fact give us the same quadratic form for mappings in the

plane, and hence either of them can be used for the computation of the 2D quasi-conformal map φ^{qc} . In practice, (4.6) is a direct summation of energies over all faces, while (4.18) only involves the boundary vertices but requires the boundary edges to be extracted and correctly oriented.

We summarize the procedure for the free-boundary quasi-conformal parameterization in Algorithm 1.

Algorithm 1: Free-boundary quasi-conformal parameterization of simply connected and multiply connected open surfaces.

Input: An open surface S_i with $p \geq 0$ inner holes and a Beltrami coefficient μ . Output: A free-boundary quasi-conformal parameterization $\varphi_i : S_i \to \mathbb{C}$.

- 1 Initial conformal parameterization step:
- **2** Compute the cotangent Laplacian matrix \mathcal{L} of \mathcal{S}_i ;
- **3** Compute the area of S_i using (4.16) (if p = 0) or (4.18) (if $p \ge 1$);
- Compute a free-boundary conformal parameterization $\varphi_i^c : \mathcal{S}_i \to \mathbb{C}$ by solving (4.17);
- 5 Quasi-conformal mapping step (if $\mu \neq 0$):
- 6 Compute the generalized Laplacian matrix \mathcal{L}_{μ} ;
- 7 Compute the area matrix using (4.6) or (4.18);
- 8 Compute a free-boundary quasi-conformal map $\varphi_i^{qc}: \varphi_i^c(\mathcal{S}_i) \to \mathbb{C}$ by solving (4.8);
- 9 The desired free-boundary quasi-conformal parameterization is given by $\varphi_i = \varphi_i^{qc} \circ \varphi_i^c$;
- 4.4. Partial welding. In the closed conformal welding problem introduced in section 3.3, we are given a homeomorphism between the boundaries of two shapes, and we need to glue the entire boundaries consistently. By contrast, in our problem we partition a mesh into several submeshes and compute the free-boundary quasi-conformal maps for them, respectively, and hence we only need to conformally glue these submeshes along the partition paths to obtain the global quasi-conformal parameterization. Since the outer boundary edges are never contained in the partition paths, the gluing paths are just continuous subsets of the boundary of the submeshes. Therefore, we need to conformally glue two submeshes with respect to a homeomorphism between two partial arcs of their boundaries. To solve this problem, we extend the partial welding method developed in [11, 12], which is a variant of the geodesic algorithm designed for handling simply connected surfaces. Below, we first briefly introduce the method for the simply connected case and then describe how we can extend it for meshes with holes.
- **4.4.1. The simply connected case.** The geodesic algorithm solves the closed welding problem by aligning the corresponding boundary points one by one. For the partial welding method, the key idea is to stop the welding process after we have exactly aligned the corresponding partial set of boundary points. Suppose we are given two sets of consecutive boundary points $\partial A = \{a_0, \ldots, a_k, \ldots, a_m\}$ and $\partial B = \{b_0, \ldots, b_k, \ldots, b_n\}$, where a_i corresponds to b_i for $i = 0, \ldots, k$. This gives rise to a correspondence function $f : \gamma_A \subset \partial A \to \gamma_B \subset \partial B$,

where γ_A and γ_B are the circular arcs formed by $\{a_0,\ldots,a_k\}$ and $\{b_0,\ldots,b_k\}$ respectively, such that $f(a_i) = b_i$ for $i = 0, \dots, k$. Now, the objective is to find two conformal maps Φ_A, Φ_B such that $\Phi_A(\gamma_A) = \Phi_B(f(\gamma_A))$. Similar to the closed welding problem, we first find mappings Ψ_A and Ψ_B to map γ_A and γ_B to the upper and lower imaginary axes, respectively, and then weld the boundary points one by one. The maps Ψ_A and Ψ_B can be realized by a halfway geodesic algorithm. The images of γ_A and γ_B under them are called *intermediate forms*. We summarize this process in Algorithm 2 as in [11].

Algorithm 2: Intermediate form transformation.

Input: A sequence of boundary points $\{z_0, \ldots, z_k, \ldots, z_n\}$ constituting a closed curve and a choice of branching.

Output: A sequence of transformed boundary points $\{Z_0, \ldots, Z_k, \ldots, Z_n\}$, where

$$Z_0, \ldots, Z_k$$
 are on the imaginary axis according to the choice of branching.
1 Let $g_1(z) = \sqrt{\frac{z-z_1}{z-z_0}}$ with the choice of branching;

2 for
$$j = 2, ..., k$$
 do

3 Compute
$$\xi_j = (g_{j-1} \circ \cdots \circ g_1)(z_j);$$

Let
$$g_j(z) = \sqrt{L_{\xi_j}(z)^2 - 1}$$
 with the choice of branching, where
$$L_{\xi_j}(z) := \frac{\frac{\operatorname{Re}(\xi_j)}{|\xi_j|^2} z}{1 + \frac{\operatorname{Im}(\xi_j)}{|\xi_j|^2} zi};$$

$$L_{\xi_j}(z) := \frac{\frac{\overline{|\xi_j|^2} z}{|\xi_j|^2} z}{1 + \frac{\operatorname{Im}(\xi_j)}{|\xi_j|^2} zi}$$

5 Set
$$g_{k+1}(z) = \frac{z}{1 - \frac{z}{g_k \circ g_{k-1} \circ \cdots \circ g_1(z_0)}};$$

6 Compute
$$Z_l = (g_{k+1} \circ \cdots \circ g_1)(z_l)$$
 for $l = 0, \dots, k, \dots, n$;

After performing the intermediate form transformation with respect to two different branches $(-1)^{1/2} = i$ and $(-1)^{1/2} = -i$, we obtain two sets of boundary points $\{A_0, \ldots, A_k, \ldots, A_k, \ldots, A_k, \ldots, A_k\}$ \ldots, A_m and $\{B_0, \ldots, B_k, \ldots, B_n\}$, all of which are in the region $\{z \in \mathbb{C} : \operatorname{Re}(z) \geq 0\}$. In particular, $\{A_0,\ldots,A_k\}$ are on the upper imaginary axis, while the corresponding $\{B_0,\ldots,B_k\}$ are on the lower imaginary axis. Next, we perform the welding step of the geodesic algorithm to weld the corresponding boundary points one by one conformally. The crucial point is the construction of the following Möbius transformation. Suppose $\alpha = ai$ and $\beta = bi$ are two corresponding points to be conformally aligned, where a>0>b. The unique Möbius transformation that maps $(\alpha, 0, \beta)$ to (i, 0, -i) is explicitly given by

$$(4.19) T_{\alpha}^{\beta}(z) = \frac{z}{\frac{-2ab}{a-b} - \frac{a+b}{a-b}zi}.$$

Consider the conformal map $z \mapsto \sqrt{z^2 + 1}$, which maps both i and -i to 0. The composition of this map and T_{α}^{β} will map both α and β to 0. Now, we apply such transformations to $\{A_0,\ldots,A_k\}$ and $\{B_0,\ldots,B_k\}$ iteratively. In the jth step, suppose we have obtained

(4.20)
$$\alpha_j = (h_{j-1}^A \circ \cdots \circ h_0^A)(A_j)$$

and

(4.21)
$$\beta_j = (h_{i-1}^B \circ \dots \circ h_0^B)(B_j).$$

Then, we define

(4.22)
$$h_j^A(z) := \sqrt{T_{\beta_j}^{\alpha_j}(z)^2 + 1}$$
, with branching $(-1)^{1/2} = i$,

and

(4.23)
$$h_j^B(z) := \sqrt{T_{\beta_j}^{\alpha_j}(z)^2 + 1}$$
, with branching $(-1)^{1/2} = -i$.

Both h_j^A and h_j^B are conformal, as they are compositions of Möbius transformations, square maps, and square root maps, and the only difference between h_j^A and h_j^B is the choice of the branching. We apply these two maps to align A_j and B_j . The images of all other points under h_j^A and h_j^B should also be updated in this iteration. After aligning all the corresponding points, we consider the following conformal closing map h_0 similar to that in the geodesic algorithm:

(4.24)
$$h_0(z) := \left(\frac{z}{1 - \frac{z}{(h_1^A \circ \dots \circ h_k^A)(\infty)}}\right)^2.$$

We may also use auxiliary points $A_{m+1} = B_{n+1} = 0$ and $A_{m+2} = B_{n+2} = \infty$ to help us perform some normalization maps to obtain more regular results as proposed in [55]. The detailed algorithm is summarized in Algorithm 3 as in [11]. We remark that while the numerical computation of the square root map is known to be error prone, it has not led to any computational issue in our experiments with different surfaces and cutting edges. In the case when such an issue occurs, choosing a smoother cutting path may be helpful.

4.4.2. The multiply connected case. In the simply connected case, when we partition the given mesh, we can ensure that the partition path is continuous. Therefore, when we apply partial welding to retrieve the entire mesh, the welding path is a continuous curve. However, this condition cannot be guaranteed for multiply connected surfaces. On the one hand, in many situations, it is natural to partition the entire mesh into several simply connected submeshes, which could reduce the computational cost and increase the stability of the algorithm. On the other hand, imposing too many restrictions on the mesh partition step could increase the difficulty and complexity of it. As a result, dealing with situations where the welding path is discontinuous, as shown in Figure 6, is inevitable.

More specifically, in Figure 6(a), we partition the given mesh into two simply connected submeshes (the blue one and the green one). It can be observed that the common boundary components of the two submeshes are two disjoint continuous arcs instead of one continuous arc. Since the inner hole is large, if we partition the surface in a way such that the inner hole is totally contained in one submesh, the welding path will contain relatively more points than the case shown in the figure, which increases the computational cost of the welding process.

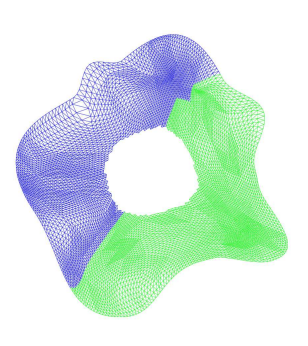
Algorithm 3: Partial welding.

Input: Two sequences of boundary points $\{a_0, \ldots, a_k, \ldots, a_m\}$ and $\{b_0,\ldots,b_k,\ldots,b_n\}$, where a_j should be aligned with b_j for $j=0,\ldots,k$. **Output**: Transformed data points $\{\tilde{a}_0, \dots, \tilde{a}_k, \dots, \tilde{a}_m\}$ and $\{\tilde{b}_0, \dots, \tilde{b}_k, \dots, \tilde{b}_n\}$ such that $\tilde{a}_i = \Phi_A(a_i), i = 1, \dots, m$, and $\tilde{b}_i = \Phi_B(b_i), i = 1, \dots, n$, for some conformal Φ_A and Φ_B , and $\tilde{a}_j = b_j, j = 0, \dots, k$.

- 1 Define auxiliary points $a_{m+1} = b_{n+1} = 0, a_{m+2} = b_{n+2} = \infty;$
- **2** Apply Algorithm 2 on $\{a_0,\ldots,a_k,\ldots,a_m,a_{m+1},a_{m+2}\}$ with branching $(-1)^{1/2}=i$ to obtain $\{A_0, \ldots, A_k, \ldots, A_m, A_{m+1}, A_{m+2}\}$. Denote the transformation by Ψ_A ;
- **3** Apply Algorithm 2 on $\{b_0,\ldots,b_k,\ldots,b_n,b_{n+1},b_{n+2}\}$ with branching $(-1)^{1/2}=-i$ to obtain $\{B_0, \ldots, B_k, \ldots, B_n, B_{n+1}, B_{n+2}\}$. Denote the transformation by Ψ_B ;
- 4 Set $h_{k-1}^A(z) := \sqrt{T_{B_{k-1}}^{A_{k-1}}(z)^2 + 1}$ with branching $(-1)^{1/2} = i$, and $h_{k-1}^B(z) := \sqrt{T_{B_{k-1}}^{A_{k-1}}(z)^2 + 1}$ with branching $(-1)^{1/2} = -i$;
- 5 for j = k 2, ..., 1 do
- Compute $\alpha_j = (h_{j+1}^A \circ \cdots \circ h_{k-1}^A)(A_j);$
- Compute $\beta_j = (h_{j+1}^B \circ \cdots \circ h_{k-1}^B)(B_j);$
- Set $h_j^A(z) := \sqrt{T_{\beta_j}^{\alpha_j}(z)^2 + 1}$ with branching $(-1)^{1/2} = i$ and $h_j^B(z) := \sqrt{T_{\beta_j}^{\alpha_j}(z)^2 + 1}$ with branching $(-1)^{1/2} = -i$;

9 Set
$$h_0(z) := \left(\frac{z}{1 - \frac{z}{(h_1^A \circ \cdots \circ h_k^A)(\infty)}}\right)^2;$$
10 Compute $\tilde{a}_l = (h_0 \circ \cdots \circ h_{k-1}^A)(A_l)$ for $l = 0, \dots, m+2;$

- 11 Compute $\tilde{b}_l = (h_0 \circ \cdots \circ h_{k-1}^B)(B_l)$ for $l = 0, \dots, n+2$;
- 12 Apply a Möbius transformation T that maps $(\tilde{a}_{m+1}, b_{n+1}, \frac{1}{2}(\tilde{a}_{m+2} + \tilde{a}_{n+2}))$ to $(-1,1,\infty)$ for all points to obtain the final result.



(a) Two submeshes



(b) More submeshes

Figure 6. Partitioning a multiply connected mesh.

Also, if the inner hole is irregular in shape, imposing the requirement that it is contained in one submesh may cause the partition method to generate a highly irregular submesh, which is undesirable. Therefore, it is important to develop a welding method for handling the situation in Figure 6(a). In the case when the partition consists of more submeshes as in Figure 6(b), we can weld the submeshes that share continuous boundary arcs and eventually reach the state in Figure 6(a). For example, we can first weld the yellow, green, and cyan submeshes in Figure 6(b) to obtain a large submesh, and then weld the red and blue ones to obtain another large submesh. This simplifies the problem to the situation in Figure 6(a). Additionally, in the case when the given mesh contains multiple holes, one can further partition it so that each of the submeshes contains exactly one hole like the mesh shown in Figure 6(a). Therefore, it suffices to focus on the case shown in Figure 6(a) and develop a partial welding method for it.

We now mathematically formulate the problem described above. Suppose $A, B \subset \overline{\mathbb{C}}$ are two Jordan domains with given orientations. Let $\gamma_A^1, \gamma_A^2 \subset \partial A$ be two disjoint arcs with the same orientation on ∂A , and let $\gamma_B^1, \gamma_B^2 \subset \partial B$ be two disjoint arcs with the same orientation on ∂B . Suppose we are given two orientation-preserving homeomorphisms $f_1: \gamma_A^1 \to \gamma_B^1$ and $f_2: \gamma_A^2 \to \gamma_B^2$. The partial welding problem aims to find two conformal maps $\Phi_A: A \to \Omega$ and $\Phi_B: B \to \mathbb{C}\backslash \overline{\Omega}$ for some domain Ω , with homeomorphic extensions to the closures, such that

(4.25)
$$\Phi_A = \Phi_B \circ f_1 \text{ on } \gamma_A^1 \text{ and } \Phi_A = \Phi_B \circ f_2 \text{ on } \gamma_A^2.$$

Recall that by Theorem 3.3, the closed welding problem is solvable if the given homeomorphism is quasi-symmetric on the real axis. To make use of this theorem, we extend the domains A and B to transform the problem to a closed welding problem. We have the following result.

Theorem 4.3. The above partial welding problem for multiply connected domains can be solved by solving a closed welding problem with a suitable extension. In particular, one can extend A and B to two larger domains \hat{A} and \hat{B} and construct the maps Φ_A and Φ_B via \hat{A} and \hat{B} .

Proof. An illustration of the construction is given in Figure 7. Suppose the starting and ending points of $\gamma_A^1, \gamma_A^2, \gamma_B^1, \gamma_B^2$ are $a_1^1, a_1^2, b_1^1, b_1^2$ and $a_2^1, a_2^2, b_2^1, b_2^2$, respectively. Since $\mathbb{C}\backslash A$ is multiply connected with one hole, we can find a curve $\gamma_A^3 \subset \mathbb{C}\backslash A$ connecting a_2^1 and a_1^2 and a curve $\gamma_A^4 \subset \mathbb{C}\backslash A$ connecting a_1^1 and a_2^2 such that γ_A^3 is not homotopic to γ_A^4 in $\mathbb{C}\backslash A$ and $\gamma_A^3 \cap \gamma_A^4 = \emptyset$. We then take \hat{A} to be the interior of $\gamma_A = \gamma_A^1 \cup \gamma_A^2 \cup \gamma_A^3 \cup \gamma_A^4$. Clearly, $A \subset \hat{A}$. Similarly, we extend B to a larger domain \hat{B} . We also extend f_1 and f_2 to a homeomorphism $f: \partial \hat{A} \to \partial \hat{B}$ such that $f\Big|_{\gamma_+^1} = f_1$ and $f\Big|_{\gamma_+^2} = f_2$.

We then find two conformal maps $\psi_{\hat{A}}: \hat{A} \to \mathbb{H}$ and $\psi_{\hat{B}}: \hat{B} \to \mathbb{C}\backslash\bar{\mathbb{H}}$, which extend continuously to homeomorphisms on the boundaries. Now, the composition map $\psi_{\hat{B}} \circ f \circ \psi_{\hat{A}}^{-1}$ is a homeomorphism from \mathbb{R} to \mathbb{R} . By Theorem 3.3, if $\psi_{\hat{B}} \circ f \circ \psi_{\hat{A}}^{-1}$ is quasi-symmetric, we can find conformal maps $\phi_{\hat{A}}: \mathbb{H} \to \Omega$ and $\phi_{\hat{B}}: \mathbb{C}\backslash\bar{\mathbb{H}} \to \mathbb{C}\backslash\bar{\Omega}$ for some Jordan domain Ω such that $\phi_{\hat{A}} = \phi_{\hat{B}} \circ f$ on \mathbb{R} . Finally, we take $\Phi_{A} = \phi_{\hat{A}} \circ \psi_{\hat{A}}|_{A}$ and $\Phi_{B} = \phi_{\hat{B}} \circ \psi_{\hat{B}}|_{B}$. It is easy to see that Φ_{A} and Φ_{B} give the desired partial welding maps.

In the discrete case, suppose we are given two set of consecutive boundary points $\partial A = \{a_0, \ldots, a_r, \ldots, a_s, \ldots, a_{s+l}, \ldots, a_m\}$ and $\partial B = \{b_0, \ldots, b_r, \ldots, b_t, \ldots, b_{t+l}, \ldots, b_n\}$, where a_i

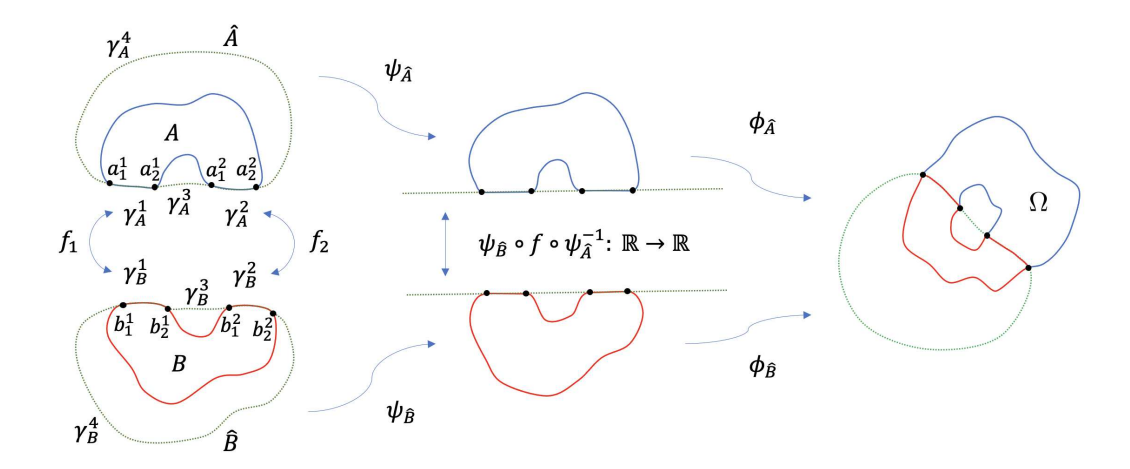


Figure 7. The theoretical construction for partial welding for multiply connected domains.

corresponds to b_i for i = 0, 1, ..., r, a_{s+i} corresponds to b_{t+i} for i = 0, 1, ..., l, and $\{a_r, ..., a_s\}$ and $\{b_r, \ldots, b_t\}$ correspond to the inner boundary of the original mesh. This gives the correspondence functions $f_1: \gamma_A^1 \to \gamma_B^1$ and $f_2: \gamma_A^2 \to \gamma_B^2$, where $\gamma_A^1, \gamma_A^2, \gamma_B^1, \gamma_B^2$ are formed by $\{a_0,\ldots,a_r\},\{a_s,\ldots,a_{s+l}\},\{b_0,\ldots,b_r\},\{b_t,\ldots,b_{t+l}\},$ respectively. Let A and B denote the polygons enclosed by $\partial A = \{a_0, \dots, a_r, \dots, a_s, \dots, a_{s+l}, \dots, a_m\}$ and $\partial B = \{b_0, \dots, b_r, \dots, b_t, \dots, a_m\}$ $\ldots, b_{t+1}, \ldots, b_n$, respectively. Our goal is to find conformal maps Φ_A and Φ_B such that $\Phi_A(\gamma_A^1) = (\Phi_B \circ f_1)(\gamma_A^1)$ and $\Phi_A(\gamma_A^2) = (\Phi_B \circ f_2)(\gamma_A^2)$. To compute the partial welding maps, we follow the idea of the theoretical construction. More specifically, we find auxiliary points $\{\bar{a}_1,\ldots,\bar{a}_k\}$ and $\{\bar{b}_1,\ldots,\bar{b}_k\}$ such that none of $\{\bar{a}_1,\ldots,\bar{a}_k\}$ is contained in the polygon A, none of $\{\bar{b}_1,\ldots,\bar{b}_k\}$ is contained in the polygon B, and $\{a_0,\ldots,a_r,\bar{a}_1,\ldots,\bar{a}_k,a_s,\ldots,a_{s+l},\ldots,a_m\}$ and $\{b_0,\ldots,b_r,\bar{b}_1,\ldots,\bar{b}_k,b_t,\ldots,b_{t+l},\ldots,b_n\}$ form two larger polygons, with the length of each edge sufficiently small, respectively. We require that the length of each edge of the new polygon be sufficiently small because it ensures a good approximation of the desired conformal map computed by the geodesic algorithm as described in [55]. We then compute the desired partial welding maps Φ_A and Φ_B with the path correspondence between $\{a_0,\ldots,a_r,\bar{a}_1,\ldots,\bar{a}_k,a_s,\ldots,$ a_{s+l} and $\{b_0,\ldots,b_r,\bar{b}_1,\ldots,\bar{b}_k,b_t,\ldots,b_{t+l}\}$. After that, we discard the polygon enclosed by $\{\Phi_A(\bar{a}_1),\ldots,\Phi_A(\bar{a}_k),\ \Phi_B(b_1),\Phi_B(b_k)\}\$ to obtain the desired multiply connected mesh. We remark that since the auxiliary points are not contained in the polygons A and B, choosing these points will not affect the final result.

Note that there are various ways to find the auxiliary points. In most cases, we can choose them to be points on the straight lines between a_r and a_s and between b_r and b_t , i.e.,

(4.26)
$$\bar{a}_i = \frac{i}{k+1} a_r + \left(1 - \frac{i}{k+1}\right) a_s$$

and

(4.27)
$$\bar{b}_i = \frac{i}{k+1} b_r + \left(1 - \frac{i}{k+1}\right) b_t$$





- (a) The given mesh partitioned into 2 submeshes
- (b) Transformed blue submesh with auxiliary path





- (c) Transformed red submesh with auxiliary path
- (d) The welded mesh

Figure 8. An illustration of the proposed partial welding method for multiply connected meshes.

for $i=1,\ldots,k$. Another possible choice is the circular arc connecting a_{r-1},a_r , and a_s . Note that the straight lines between a_r and a_s and between b_r and b_t generally work well for the partial welding method. More specifically, suppose the original mesh is partitioned into two submeshes as shown in Figure 8(a). The line connecting the starting and ending points a_r and a_s is in the inner hole of the mesh in most cases. As conformal maps and quasi-conformal maps with small $|\mu|$ tend to preserve the local geometry of the mesh, the line connecting a_r and a_s should lie outside the transformed submeshes if the distortion is small enough, as shown in Figure 8(b)–(c). The partial welding method can then be applied to weld the two submeshes as shown in Figure 8(d). For some extreme cases where the straight lines do not lie outside the submeshes, we may apply some other path-finding algorithms, such as those in [25, 76], to get the auxiliary points. The proposed partial welding method is summarized in Algorithm 4.

4.5. Parallel Koebe's iteration. As introduced in section 3.5, when we perform the Koebe's iteration for a domain R whose complements are K_1, K_2, \ldots, K_n , in each iteration, we normalize the iteration map f_j at ∞ such that $f_j(z) = z + O(\frac{1}{z})$. This plays an essential role in ensuring the convergence of the Koebe's iteration. Intuitively, with f_j normalized at ∞ , it only changes the region near K_j while being close to the identity map (possibly with a rotation) locally for points far away from K_j . Moreover, suppose in the (j-1)th iteration we have transformed the inner boundary of K_{j-1} into a circle. Then, in the jth iteration, the transformed inner boundary will still be similar to a circle if K_{j-1} is far away from K_j . Computationally, the normalization step is incorporated as the last step of the geodesic algorithm as in [55]. Figure 9 shows an example of the effect, from which it can be observed that the region near the curve is significantly changed under the map, while the region far away from it is only rotated but not distorted locally. This motivates us to design a parallelizable version

Algorithm 4: Partial welding for multiply connected meshes.

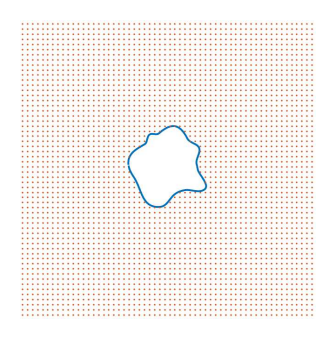
Input: Two sequences of boundary points $\partial A = \{a_0, \dots, a_r, \dots, a_s, \dots, a_{s+l}, \dots, a_m\}$ and $\partial B = \{b_0, \dots, b_r, \dots, b_t, \dots, b_{t+l}, \dots, b_n\}$, where a_i are to be aligned with b_i for $i = 0, \dots, r$, a_{s+i} are to be aligned with b_{t+i} for $i = 0, 1, \dots, l$, and $a_r, \dots, a_s, b_r, \dots, b_t$ are taken from the inner boundaries.

Output: Conformally transformed points $\{\tilde{A}_0, \ldots, \tilde{A}_r, \ldots, \tilde{A}_s, \ldots, \tilde{A}_{s+l}, \ldots, \tilde{A}_m\}$ and $\{\tilde{B}_0, \ldots, \tilde{B}_r, \ldots, \tilde{B}_t, \ldots, \tilde{B}_{t+l}, \ldots, \tilde{B}_m\}$ such that $\tilde{A}_i = \tilde{B}_i$ for $i = 0, \ldots, r$, $\tilde{A}_{s+i} = \tilde{B}_{t+i}, i = 0, 1, \ldots, l$, and the transformed points form a multiply connected polygon.

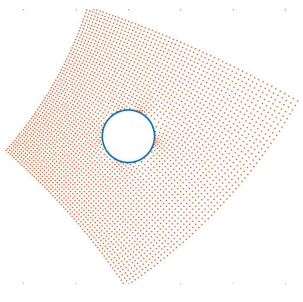
1 Find auxiliary points $\bar{a}_1, \ldots, \bar{a}_k$ and $\bar{b}_1, \ldots, \bar{b}_k$ such that they are not in the polygons A and B, respectively. Also, $\{a_0, \ldots, a_r, \bar{a}_1, \ldots, \bar{a}_k, a_s, \ldots, a_{s+l}, \ldots, a_m\}$ and $\{b_0, \ldots, b_r, \bar{b}_1, \ldots, \bar{b}_k, b_t, \ldots, b_{t+l}, \ldots, b_n\}$ form two larger polygons;

2 Apply the partial welding algorithm (Algorithm 3) with path correspondences $\{a_0, \ldots, a_r, \bar{a}_1, \ldots, \bar{a}_k, a_s, \ldots, a_{s+l}\}$ and $\{b_0, \ldots, b_r, \bar{b}_1, \ldots, \bar{b}_k, b_t, \ldots, b_{t+l}\}$ to update ∂A and ∂B ;

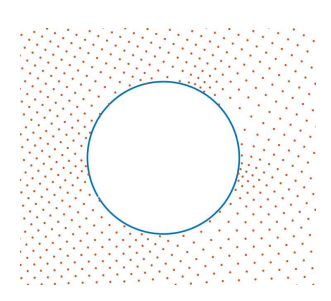
3 The new coordinates of ∂A and ∂B give the desired map.



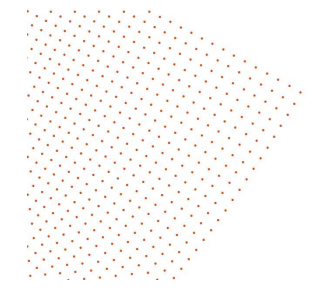
(a) The original curve and its exterior



(b) The computed conformal map



(c) Zoom-in of the region near the circle



(d) The map causes a rotation far away from the circle

Figure 9. The conformal map from the exterior of a curve to the exterior of a circle computed using the geodesic algorithm.

of the Koebe's iteration method for our parallel quasi-conformal parameterization problem.

Let S be the input multiply connected mesh with exactly k inner holes. Suppose S is partitioned into m submeshes S_1, \ldots, S_m , where each is either simply connected or multiply

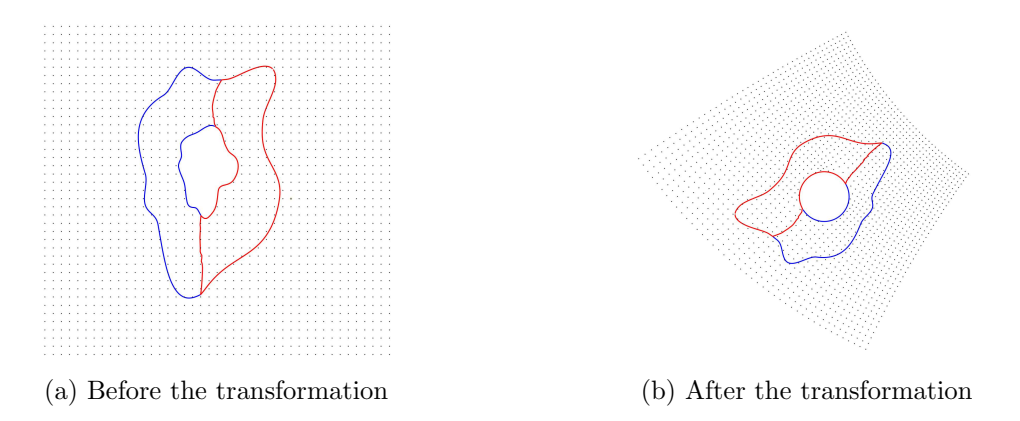
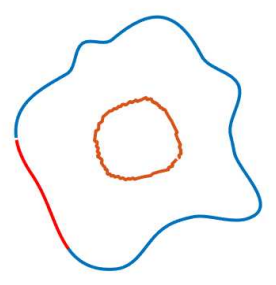


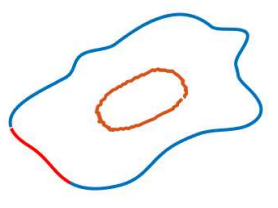
Figure 10. Transforming the inner boundary of a one-hole submesh S_j into a circle using the geodesic algorithm under normalization.

connected with one inner hole, and the free-boundary quasi-conformal parameterizations of them obtained using Algorithm 1 are $\varphi_1, \ldots, \varphi_m$. Instead of merging all flattened submeshes and performing the traditional Koebe's iteration on the entire mesh directly, we apply the geodesic algorithm to weld some of the submeshes so that each of the k holes is contained in one of $\varphi_i(\mathcal{S}_i)$ or a welded larger subdomain. We then transform the inner boundary \mathcal{H}_i of each subdomain $\varphi_i(\mathcal{S}_i)$ (or a welded larger subdomain) into a circle in parallel. More explicitly, we find a normalized conformal map $\Phi_j: \mathbb{C}\backslash\mathcal{H}_j \to \mathbb{C}\backslash B(0,1)$ satisfying $\Phi_j(\partial\mathcal{H}_j) =$ $S(0,1), \Phi_i(\infty) = \infty$, and $\Phi_i(a_0) = 0$ for some point a_0 on $\partial \mathcal{H}_i$, where B(0,1) denotes the unit ball and S(0,1) denotes the unit circle. All the boundary points and welding paths related to $\varphi_i(\mathcal{S}_i)$ should be updated. Figure 10 shows an example of the transformation. Since the transformations of all \mathcal{H}_i into circles are independent, in practice they can be computed by different processors in a parallel manner. After computing all transformations, we obtain the updated boundaries of the submeshes S_1, \ldots, S_k, \ldots , where each is either simply connected or multiply connected with one circular hole. We can then perform the remaining welding steps to get the entire boundaries. Figure 11 shows an example of the computation, in which we handle the two submeshes with one hole in (a) and (b) in parallel to get the results in (c) and (d), and then weld them to get the result in (e). Note that the normalization step of partial welding tends to preserve the circular shapes of all inner boundaries. As for the outer boundary of the entire mesh, we can apply the geodesic algorithm to transform it into a circle after all the welding steps. This completes our parallel Koebe's iteration method. We remark that the interior of the submeshes does not need to be updated throughout the process, as we will only utilize the boundary points of them to compute the desired parameterization later.

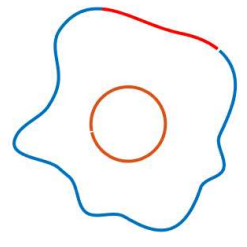
To see the advantage of the proposed parallel Koebe's iteration, note that the complexity of the geodesic algorithm is $O(n_b n_t)$, where n_b is the number of boundary points that determine the map and n_t is the total number of points we want to update using the map. We now consider the computational cost of the traditional (nonparallel) Koebe's iteration method and our proposed parallel Koebe's iteration. To transform the inner boundary of each subdomain with one hole into a circle using the geodesic algorithm, the number n_b is the number of boundary points of such a subdomain in both versions of the Koebe's iteration. As for the



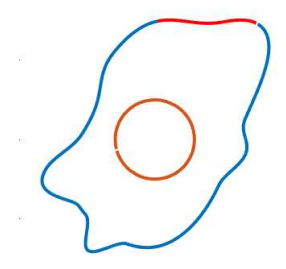
(a) The first multiply connected submesh



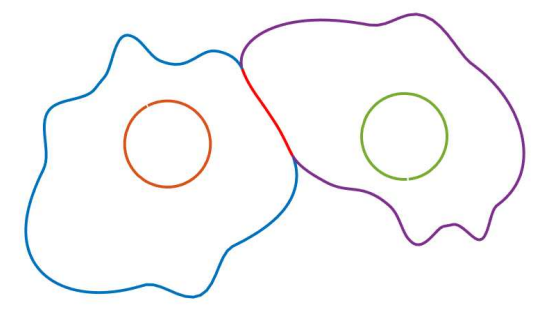
(b) The second multiply connected submesh



(c) Transforming the inner boundary of (a) into a circle



(d) Transforming the inner boundary of (b) into a circle



(e) The inner boundaries remain close to circles after partial welding

Figure 11. An illustration of the parallel Koebe's iteration.

number n_t , if we perform the traditional Koebe's iteration on the entire welded shape, n_t will be the total number of boundary points of the submeshes. By contrast, in the parallel Koebe's iteration, we only need to update the new coordinates of the boundary points of each submesh in parallel, and hence n_t is just the number of boundary points of each submesh for computing each map. Therefore, the computational cost can be greatly reduced in the parallel Koebe's iteration by utilizing multiple processors, especially if the mesh S has many inner boundaries.

We remark that the parallel Koebe's iteration method is developed based on the observation that the transformed circles remain close to circles under the subsequent welding maps, and hence the result obtained by the algorithm is only an approximation of the desired Riemann mapping in theory. To ensure that all boundaries are perfectly circular, one needs to repeat the Koebe's iteration infinitely many times so that the result will converge to the desired Riemann mapping as guaranteed by Theorem 3.5. Nevertheless, in practice we find that the results produced by the proposed parallel Koebe's iteration algorithm without repeating the iterations are already satisfactory, with all holes being very close to perfect circles. In the case when the precision of the circularity of the holes is required to be particularly high, one can repeat the iterations several times to further improve the circularity.

4.6. Obtaining the global quasi-conformal parameterization. After getting the updated boundary conditions for all submeshes from the above procedures, we compute the desired free-boundary quasi-conformal parameterization of each one. Suppose the boundary of each initially flattened submesh $\varphi_i(\mathcal{S}_i)$ is \mathcal{B}_i , where $i=1,\ldots,m$. After the steps of partial welding and parallel Koebe's iteration, we obtain the updated boundary $\tilde{\mathcal{B}}_i$ for each submesh. Now, we use the updated boundary to obtain the desired quasi-conformal parameterization for each submesh. Since a conformal map is harmonic, we can solve the following Laplace equation for each flattened subdomain $\varphi_i(\mathcal{S}_i)$ to obtain a conformal map $\Phi_i: \varphi_i(\mathcal{S}_i) \to \mathbb{C}$:

$$(4.28) \Delta \Phi_i = 0, \ \Phi_i|_{\mathcal{B}_i} = \tilde{\mathcal{B}}_i.$$

Note that since the computation for each submesh is independent, this step is highly parallelizable. We can further reduce the quasi-conformal distortion of each Φ_i by composing Φ_i with a quasi-conformal map, where the Beltrami coefficient is computed using the composition formula (3.4) as suggested by [18]. Also, note that there is no theoretical guarantee of the bijectivity of the harmonic maps if the updated boundaries are nonconvex. Nevertheless, as mentioned in [11], the optional quasi-conformal composition step can also be used to ensure the bijectivity of the mappings. Now, since Φ_i is conformal, the Beltrami coefficient of the composition map $\Phi_i \circ \varphi_i : \mathcal{S}_i \to \mathbb{C}$ is the same as that of φ_i , which is obtained based on the input Beltrami coefficient μ . In other words, this step of solving the Laplace equation for each submesh ensures the consistency of the boundaries of all submeshes without affecting their quasi-conformality. Finally, all mapping results $\Phi_i \circ \varphi_i$, $i = 1, \ldots, m$, together form the desired global quasi-conformal parameterization $\Phi : \mathcal{S} \to \mathbb{C}$, with the Beltrami coefficient of Φ being μ and all k holes of $\Phi(\mathcal{S})$ very close to circles. Our parallelizable global quasi-conformal mapping (PGQCM) method for multiply connected surfaces is summarized in Algorithm 5.

The convergence of the PGQCM algorithm is guaranteed by the following theorem.

Theorem 4.4. Let S be a multiply connected open surface and μ be a prescribed Beltrami coefficient. If the Koebe's iteration is repeated infinitely many times, the map $\Phi: S \to \mathbb{C}$ obtained by the PGQCM algorithm converges to the quasi-conformal Riemann mapping in Theorem 3.6, where all boundaries of $\Phi(S)$ are circular and the Beltrami coefficient of Φ is μ .

Proof. Note that the circularity of the holes is ensured by the convergence of the Koebe's iteration in Theorem 3.5. Also, the error in the Beltrami coefficient of the map can be corrected by composing a quasi-conformal map using the composition formula as introduced in [18], and hence one can ensure that the Beltrami coefficient of Φ is equal to the prescribed μ .

Altogether, the novel combination of the free-boundary local parameterization of the submeshes, the partial welding method, and the parallel Koebe's iteration significantly improve **Algorithm 5:** Parallelizable global quasi-conformal mapping for multiply connected surfaces (PGQCM).

Input: A multiply connected surface mesh S = (V, F) with k inner holes, and a prescribed Beltrami coefficient μ , and a partition of S into m submeshes $S_i = (V_i, F_i), i = 1, ..., m$.

Output: A global quasi-conformal parameterization $\Phi : \mathcal{S} \to \mathbb{C}$.

- 1 for i = 1, ..., m do
- **2** Apply Algorithm 1 to obtain the free-boundary parameterization $\varphi_i : \mathcal{S}_i \to \mathbb{C}$;
- **3** Perform partial welding on $\varphi_i(S_i)$ using Algorithm 4 to get \tilde{S}_j , j = 1, ..., k, ..., such that each is simply connected or has only one hole and each of the k holes is contained in one of \tilde{S}_j ;
- 4 Apply the geodesic algorithm to transform the inner boundaries of all one-hole submeshes into circles:
- 5 Perform partial welding to ensure the consistency of all boundaries of the submeshes;
- 6 Apply the geodesic algorithm to transform the outer boundary into a circle;
- 7 (Optional) Further perform the Koebe's iteration to improve the circularity of the inner holes;
- 8 for i = 1, ..., m do
- Solve the Laplace equation $\Delta \Phi_i = 0$ with the updated boundary conditions for $\varphi_i(\mathcal{S}_i)$;
- (Optional) Compose the map with a quasi-conformal map to further reduce the quasi-conformal distortion and ensure the bijectivity;
- 11 The maps $\Phi_i \circ \varphi_i : \mathcal{S}_i \to \mathbb{C}, i = 1, ..., m$, together form the desired map $\Phi : \mathcal{S} \to \mathbb{C}$;

the computational efficiency of the global quasi-conformal parameterization of multiply connected surfaces. Furthermore, for some very dense meshes, traditional global parameterization methods may fail due to insufficient memory size of the computing machines for solving extremely large systems of equations. By contrast, our proposed PGQCM algorithm can effectively handle any dense mesh, as it does not require solving any equations for the global mesh. Instead, we can partition the input mesh into multiple submeshes such that each is small enough for the computing machine to compute the free-boundary quasi-conformal parameterization. After that, we can perform the partial welding and the parallel Koebe's iteration to weld and update the boundaries and to finally solve the Laplace equation for each submesh with the updated boundary conditions to get the desired mapping for each, thereby yielding the desired global quasi-conformal parameterization of the dense mesh. Note that the accuracy of the welding maps is theoretically ensured as described in [55]. In the experiments presented in the following section, one can see that the proposed PGQCM method is not only more efficient but also more accurate than the existing methods, especially for dense meshes.

5. Experiments. Our proposed algorithm is implemented in MATLAB using the Parallel Computing Toolbox to perform the parallel computation in our algorithm. The sparse linear systems are solved using the backslash operator (\) in MATLAB. The numerical calculations

are done using the default 16-digit precision in MATLAB. All experiments are performed on a MacBook Pro with 2.3 GHz 8-Core Intel Core i9 CPU and 16 GB RAM. Various synthetic and real multiply connected mesh models from [7, 28, 29] are used for assessing the performance of our proposed algorithm.

5.1. Error estimate. For a given multiply connected surface $S = (V, \mathcal{F})$ and a prescribed piecewise constant Beltrami coefficient μ defined on each face of S, let $\Phi : S \to \mathbb{C}$ be the computed quasi-conformal parameterization. We first measure the error e_T between the Beltrami coefficient μ_{Φ} of the resulting map Φ and the ground truth Beltrami coefficient μ on each face $T \in \mathcal{F}$,

(5.1)
$$e_T = (\mu_{\Phi} - \mu)|_T,$$

where $\mu_{\Phi}|_{T}$ is the Beltrami coefficient of the linear map from $T=[v_i,v_j,v_k]$ to $\Phi(T)=[\Phi(v_i),\Phi(v_j),\Phi(v_k)]$. We can then compute the mean absolute error

$$(5.2) e = \max_{T \in \mathcal{F}} |e_T|.$$

Note that we do not adopt the relative error $\frac{|e_T|}{|\mu|_T|}$ or $\frac{|e_T|}{\text{mean}(|\mu|)}$ here because if the ground truth μ is identically zero, i.e., the desired parameterization is conformal, then the relative error will be ∞ no matter how small e_T and hence will not be a good measure. Since the Beltrami coefficient effectively captures the local geometric distortion of the parameterization, a small mean absolute error e indicates that the conformality distortion between the desired parameterization and the computed parameterization is very small. Mathematically, this can be seen from the composition formula of Beltrami coefficients in (3.4). If we denote the ground truth quasi-conformal map as $\Psi: \mathcal{S} \to \mathbb{C}$, then we have

(5.3)
$$\mu_{\Psi^{-1}}(\Psi(z_0)) = -\mu_{\Psi}(z_0) \frac{\Psi_z(z_0)}{\bar{\Psi}_z(z_0)}$$

and

$$(5.4) \qquad \mu_{\Phi \circ \Psi^{-1}}(\Psi(z_0)) = \frac{\mu_{\Psi^{-1}} + (\mu_{\Phi} \circ \Psi^{-1}) \frac{\bar{\Psi}_z^{-1}}{\bar{\Psi}_z^{-1}}}{1 + \bar{\mu}_{\Psi^{-1}}(\mu_{\Phi} \circ \Psi^{-1}) \frac{\bar{\Psi}_z^{-1}}{\bar{\Psi}_z^{-1}}} (\Psi(z_0)) = \frac{\Psi_z(z_0)(\mu_{\Phi}(z_0) - \mu_{\Psi}(z_0))}{\bar{\Psi}_z(z_0)(1 - \bar{\mu}_{\Psi}(z_0)\mu_{\Phi}(z_0))}.$$

Consequently, we have

(5.5)
$$\left| \mu_{\Phi \circ \Psi^{-1}}(\Psi(z_0)) \right| \le C \left| \mu_{\Phi}(z_0) - \mu_{\Psi}(z_0) \right|,$$

where C is a constant depending on Φ and Ψ . This shows that when μ_{Φ} and μ_{Ψ} are close enough, the composition map $\Phi \circ \Psi^{-1}$ is close to conformal, and hence the errors e_T and e we adopt are good measurements of the error in the Beltrami coefficients.

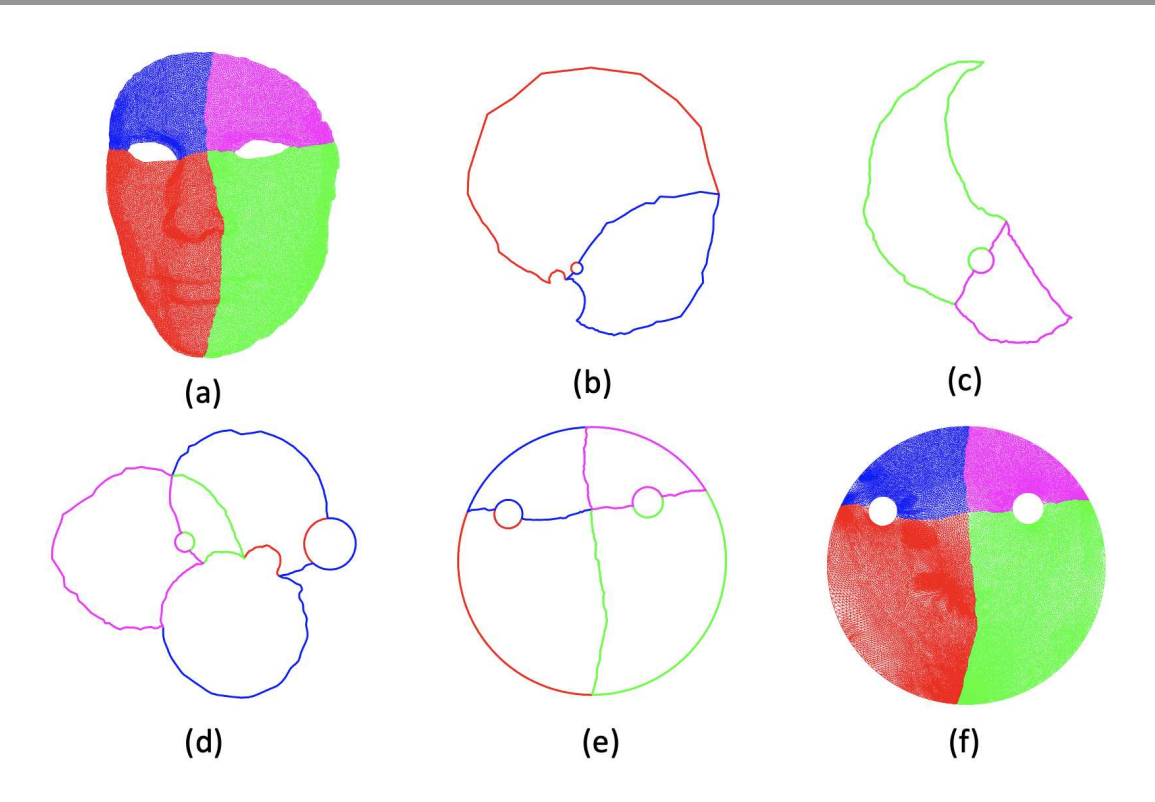


Figure 12. Parameterizing a multiply connected mesh with two holes using our PGQCM algorithm.

5.2. Example 1: A multiply connected face mesh with two inner holes. We first test our proposed PGQCM algorithm on a multiply connected face mesh with two inner holes as shown in Figure 12. Figure 12(a) shows the face mesh partitioned into four submeshes. We compute the free-boundary quasi-conformal parameterization for each mesh and then perform the partial welding and Koebe's iteration. Specifically, by welding the boundaries of the red submesh and the blue submesh together based on their partial correspondence and then transforming the inner boundary of the welded mesh into a circle, we obtain the updated boundary conditions as shown in Figure 12(b). Similarly, we obtain the updated boundary conditions of the green submesh and the magenta submesh as shown in Figure 12(c) by welding them together and transforming the inner boundary into a circle. After that, we weld the two welded shapes in Figure 12(b)-(c) according to their boundary correspondence and obtain the updated boundary conditions in Figure 12(d). It can be observed that the two inner holes remain close to circles, which demonstrates the efficacy of our parallel Koebe's iteration. Now, since the outer boundary of the updated shape is not circular, we perform the geodesic algorithm to transform it into a circle with other points lying inside it as shown in Figure 12(e). Finally, with the updated boundary conditions, we can compute the quasiconformal parameterization for each submesh and obtain the global parameterization as shown in Figure 12(f). Table 1 records the mean absolute error between the prescribed Beltrami coefficient and the Beltrami coefficient of the parameterization result for each submesh, from which we see that the error is very small for all submeshes.

Table 1
Mean absolute error in Beltrami coefficients μ for each submesh in Figure 12.

Submesh	Error e
Submesh 1	0.0130
Submesh 2	0.0106
Submesh 3	0.0074
Submesh 4	0.0088

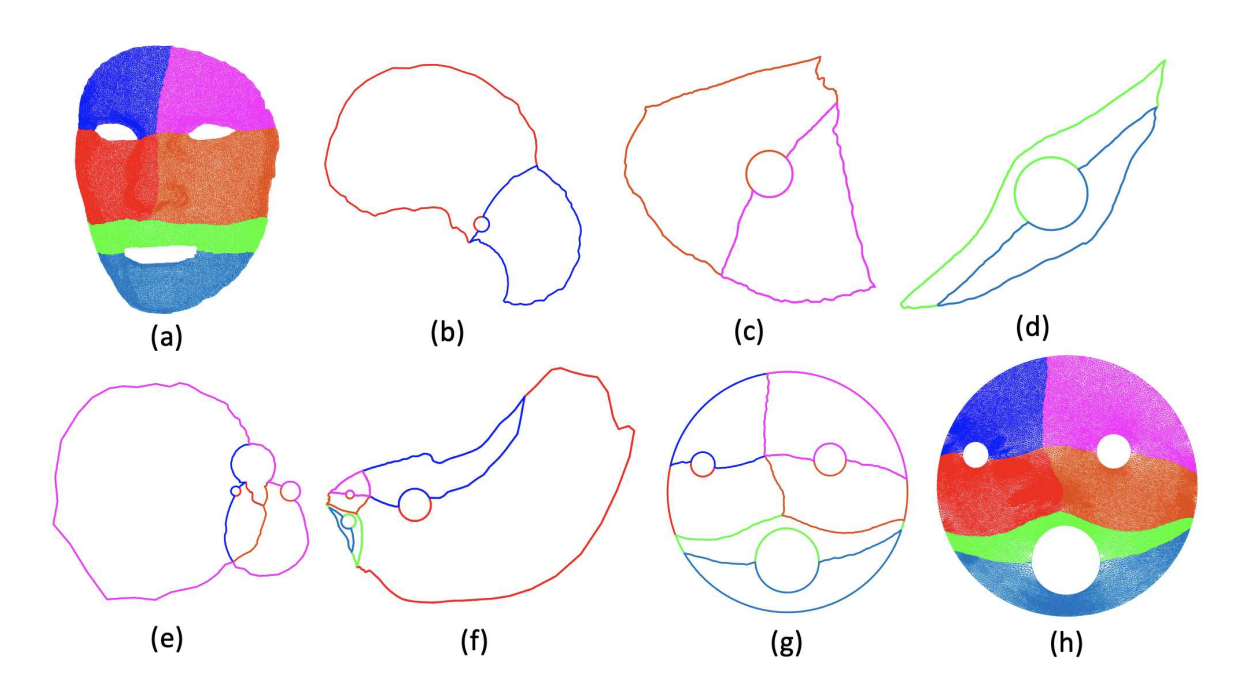


Figure 13. Parameterizing a multiply connected mesh with three holes using our PGQCM algorithm.

5.3. Example 2: A multiply connected face mesh with three inner holes. We then test our algorithm on another multiply connected face mesh with three inner holes as shown in Figure 13. Figure 13(a) shows the face mesh partitioned into six submeshes. We first compute the free-boundary quasi-conformal parameterization of each submesh, respectively. Then, as shown in Figure 13(b)–(d), we weld three pairs of submesh boundaries and transform the inner boundaries of the results into circles. After that, we continue to perform welding to obtain the global mapping of the boundaries as shown in Figure 13(e)–(f). It can be observed that the inner boundaries remain very close to circles under the map. We then apply the geodesic algorithm to transform the outer boundary into a circle as shown in Figure 13(g). Finally, we solve the Laplace equation for each submesh with the updated boundary condition to obtain the global quasi-conformal parameterization as shown in Figure 13(h). The mean absolute error in the Beltrami coefficients is recorded in Table 2, from which we can again see that the parameterization is very accurate.

5.4. Example 3: A synthetic mesh with four inner holes. We now consider parameterizing a synthetic multiply connected mesh with three inner holes as shown in Figure 14.

Table 2
Mean absolute error in Beltrami coefficients μ for each submesh in Figure 13.

Submesh	Error e
Submesh 1	0.0213
Submesh 2	0.0107
Submesh 3	0.0139
Submesh 4	0.0118
Submesh 5	0.0131
Submesh 6	0.0087

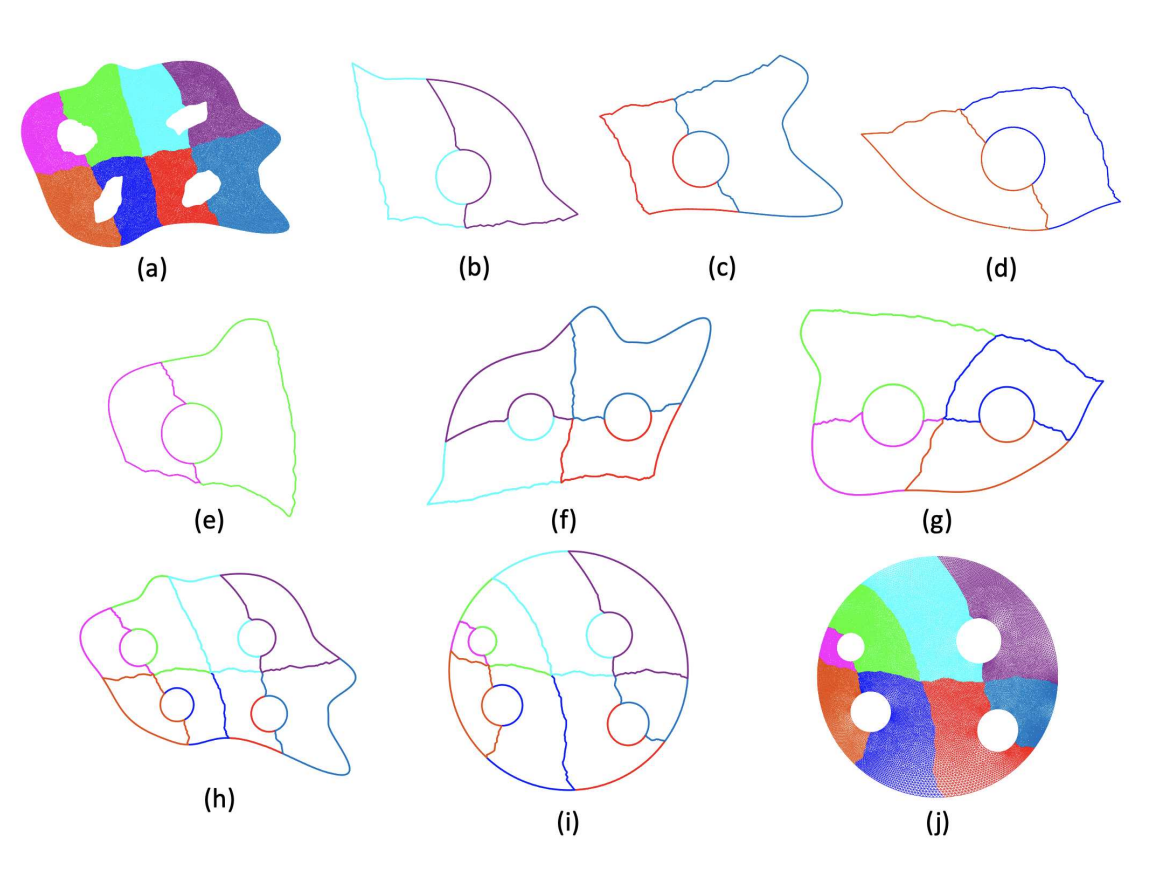


Figure 14. Parameterizing a multiply connected mesh with four holes using our PGQCM algorithm.

Figure 14(a) shows the original mesh partitioned into eight submeshes. After computing the free-boundary quasi-conformal parameterization for each submesh, we weld four pairs of submesh boundaries and transform the inner boundary of each into a circle as shown in Figure 14(b)–(e). Then, we weld the results of Figure 14(b)–(c) into Figure 14(f) and those of Figure 14(d)–(e) into Figure 14(g). It can be observed that the inner boundaries are still very close to circles after the welding step. In Figure 14(h), we show the global boundary condition obtained by welding the results of Figure 14(f)–(g). We then transform the outer boundary into a circle to obtain the result in Figure 14(i). Finally, we solve that Laplace equation for each submesh with the updated boundary condition to obtain the global parameterization in

Table 3
Mean absolute error in Beltrami coefficients μ for each submesh in Figure 14.

Submesh	Error e
Submesh 1	0.0064
Submesh 2	0.0071
Submesh 3	0.0089
Submesh 4	0.0135
Submesh 5	0.0054
Submesh 6	0.0117
Submesh 7	0.0056
Submesh 8	0.0038

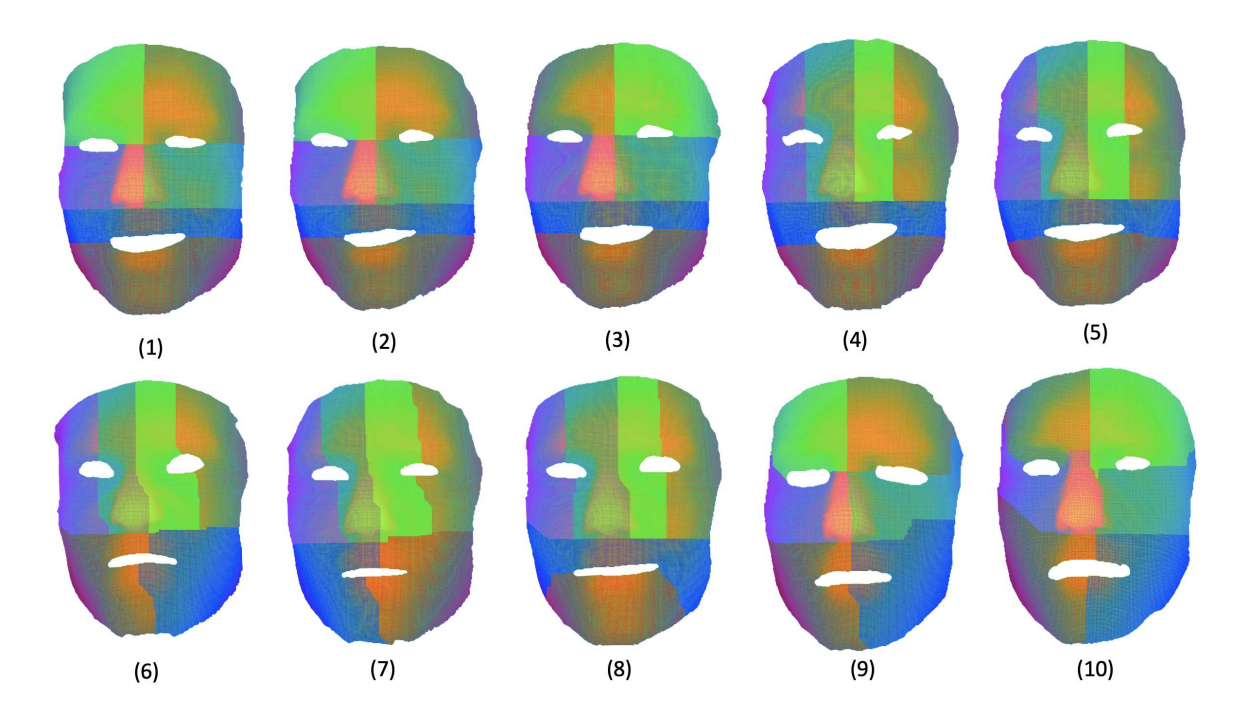


Figure 15. The 10 3D scanned human face meshes from [29] with dynamic facial expression changes considered in our experiment. Each mesh is a multiply connected mesh with four inner holes. Different subdomains are highlighted in different colors.

Figure 14(j). As shown in Table 3, the mean absolute error in the Beltrami coefficients is very small for all submeshes.

5.5. Example 4: 3D scanned human faces. To further assess the performance of our algorithm, we consider 10 3D scanned human face meshes from [29] with dynamic facial expression changes, where the eyes and mouth of the surfaces are removed so that each surface is a multiply connected surface with three inner holes (see Figure 15). We compute the conformal parameterization of the surfaces using the proposed PGQCM method (see Figure 16). From the mean absolute error in the Beltrami coefficients for the 10 meshes in Table 4, we can see that our method consistently achieves very low conformal distortion.

proposed PGQCM method.

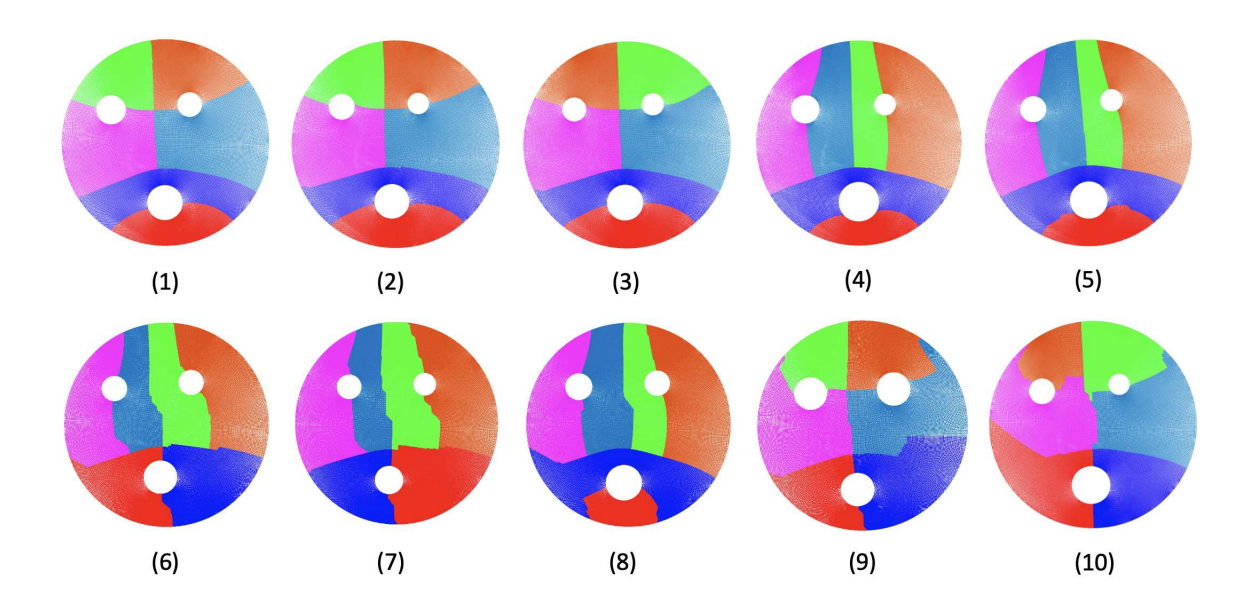


Figure 16. The conformal parameterization of the human face meshes in Figure 15 using our PGQCM algorithm.

Table 4

Mean absolute error in Beltrami coefficients μ for each human face mesh in Figure 15.

Face 1	Face 2	Face 3	Face 4	Face 5
0.0053	0.0053	0.0053	0.0055	0.0051
Face 6	Face 7	Face 8	Face 9	Face 10
0.0051	0.0052	0.0052	0.0054	0.0049

5.6. Comparison between our proposed method and other parameterization methods. After demonstrating the effectiveness of our proposed PGQCM method using various examples, we compare our method with other existing conformal and quasi-conformal parameterization methods in terms of the accuracy and efficiency. For each example, we manually prescribe a set of cutting edges to partition the surface into several submeshes and apply our

We first compare our proposed method with the QCMC iterative method for quasi-conformal parameterization [34]. As shown in Table 5, our method is significantly faster than the QCMC method by over 95% on average for coarse and moderately dense meshes. For dense meshes, either our method is nearly 100 times faster or the QCMC method fails to compute the desired mapping. This can be explained by the use of the divide-and-conquer strategy with parallelization in our algorithm. Also, the mean absolute error in the Beltrami coefficients of our method is generally much smaller than that of QCMC, especially for moderate and dense meshes. The experiments show that our method is more advantageous for computing quasi-conformal parameterization of multiply connected surfaces.

Next, we compare our proposed method with the recently developed PACM algorithm [7].

Table 5

Comparison between PGQCM and QCMC [34] for quasi-conformal parameterization of multiply connected open surfaces in terms of the computational time and the mean absolute error in the Beltrami coefficients.

Mesh	# vertices	PGQCM		QCMC		
Mesn	# vertices	# submeshes	Time (s)	Error e	Time (s)	Error e
Amoeba 1	7322	2	0.1980	0.0389	7.8300	0.0420
Amoeba 2	27755	8	1.0229	0.0082	35.5800	0.0281
Alex	13969	4	0.6515	0.0129	14.5116	0.0255
David 1	47550	4	0.9883	0.0108	28.4376	0.0234
David 2	48853	6	0.8251	0.0083	28.8781	0.0225
Face	518890	6	14.5266	0.0014	1233.2295	0.0139
Stripe	720150	6	21.6211	0.0024	Failed	N/A
Catenary	1113041	6	37.8381	0.0015	Failed	N/A

Table 6

Comparison between PGQCM and PACM [7] for conformal parameterization of multiply connected open surfaces in terms of the computational time and the mean absolute error in the Beltrami coefficients.

Mesh	# vertices	PGQCM			PACM	
Mesii	# vertices	# submeshes	Time (s)	Error e	Time (s)	Error e
Amoeba 1	7322	2	0.1899	0.0173	0.5232	0.0106
Amoeba 2	27755	8	1.0185	0.0078	5.1781	0.0044
Alex	13969	4	0.6559	0.0127	2.5095	0.0218
David 1	47550	4	0.8107	0.0106	3.9559	0.0213
David 2	48853	6	0.7783	0.0079	3.3490	0.0086
Face	518890	6	11.6979	0.0013	100.2848	0.0041
Stripe	720150	6	17.7237	0.0029	214.6671	0.0198
Catenary	1113041	6	31.8079	0.0014	349.2447	0.0186

In particular, since the PACM method only works for the conformal parameterizations of multiply connected surfaces, here we set the target Beltrami coefficient in our algorithm to be $\mu \equiv 0$ and compute conformal parameterizations for the comparison. As shown in Table 6, our method is faster than the PACM method by over 80% on average. Also, the mean absolute error in the Beltrami coefficients of our method is generally much smaller than that of PACM for moderate and dense meshes. This shows that our method is useful not only for quasiconformal parameterization but also for conformal parameterization of multiply connected surfaces.

To further explain the significant improvement in the computational efficiency achieved by our method, note that computing a free-boundary quasi-conformal map for a global mesh requires solving a large sparse linear system. More specifically, for the global mapping of a triangle mesh with N vertices, one needs to solve a linear system of size $2N \times 2N$. However, if we partition the mesh into k submeshes of the same size, we only need to solve k much smaller linear systems of size $\frac{2N}{k} \times \frac{2N}{k}$. Suppose the original computation cost is C. By partitioning the mesh into submeshes, we reduce the cost to $\frac{C}{k^{1/2}}$. Since partitioning the surface enables us to apply parallel computing to compute the parameterization, the computational time can be further reduced by a large extent. Also, when the mesh size is extremely large, other existing global mapping methods may fail due to the extremely large linear systems involved. By contrast, by partitioning the surface, in our method we only need to handle smaller linear

Table 7

Assessing the circularity of the holes under multiple cycles of the parallel Koebe's iteration. For each surface, different numbers of cycles N and the corresponding average hole circularity c are recorded.

Mesh	Hole circularity c after N cycles			/ cycles
Mesii	N = 1	N=2	N=5	N = 10
Amoeba 1	0.9996	0.9997	0.9997	0.9997
Amoeba 2	0.9994	0.9997	0.9997	0.9997
David 2	0.9992	0.9992	0.9992	0.9992
Figure 17	0.9964	0.9997	0.9997	0.9997

systems, which are much easier to solve. Note that we also need to take the additional computation cost of welding into account when analyzing the total computational cost. However, since the welding step only involves the boundary points, and the complexity of the geodesic algorithm is O(mn) where m is the number of points that determine the map and n is the number of points we want to update, the computational cost of the welding step is considerably less than that of the quasi-conformal parameterization step. Additionally, as discussed in detail in section 4.5, partitioning the mesh allows us to perform the parallel Koebe's iteration, which also helps reduce the total computational cost. Overall, our method greatly accelerates the computation of conformal and quasi-conformal parameterizations for multiply connected surfaces. We remark that the performance of the parallel computation would be affected by the number of submeshes and CPU cores used. Similar to the decrease in marginal utility of further submesh refinement observed in our prior conformal parameterization work [11], the results in Tables 5 and 6 may be different if different setups are used.

5.7. Performing more cycles of the Koebe's iteration. As described previously, our proposed parallel Koebe's iteration method can produce satisfactory results with all holes being highly circular after one cycle of the Koebe's iteration for most surfaces in practice. To demonstrate this, here we consider running more cycles of the Koebe's iteration in line 7 of Algorithm 5 and assess the circularity of the holes. More specifically, by the isoperimetric inequality, the length L and the area A of any closed plane curve must satisfy

$$(5.6) L^2 \ge 4\pi A,$$

and the equality holds if and only if the curve is a circle. Therefore, for a surface with k inner holes, we can quantify the overall hole circularity after a certain number of cycles of the parallel Koebe's iteration by

$$(5.7) c = \text{mean} \frac{4\pi A_i}{L_i^2},$$

where L_i and A_i are the length and area of the *i*th hole, respectively, i = 1, ..., k. From the result in Table 7, it can be observed that performing one cycle of Koebe's iteration already yields a satisfactory result with $c \approx 1$, and running multiple cycles can only marginally improve the circularity for most surfaces in practice.

We remark that for surfaces with very large holes, the improvement in the hole circularity by performing multiple cycles of Koebe's iteration may be more significant. In section 4.5, we

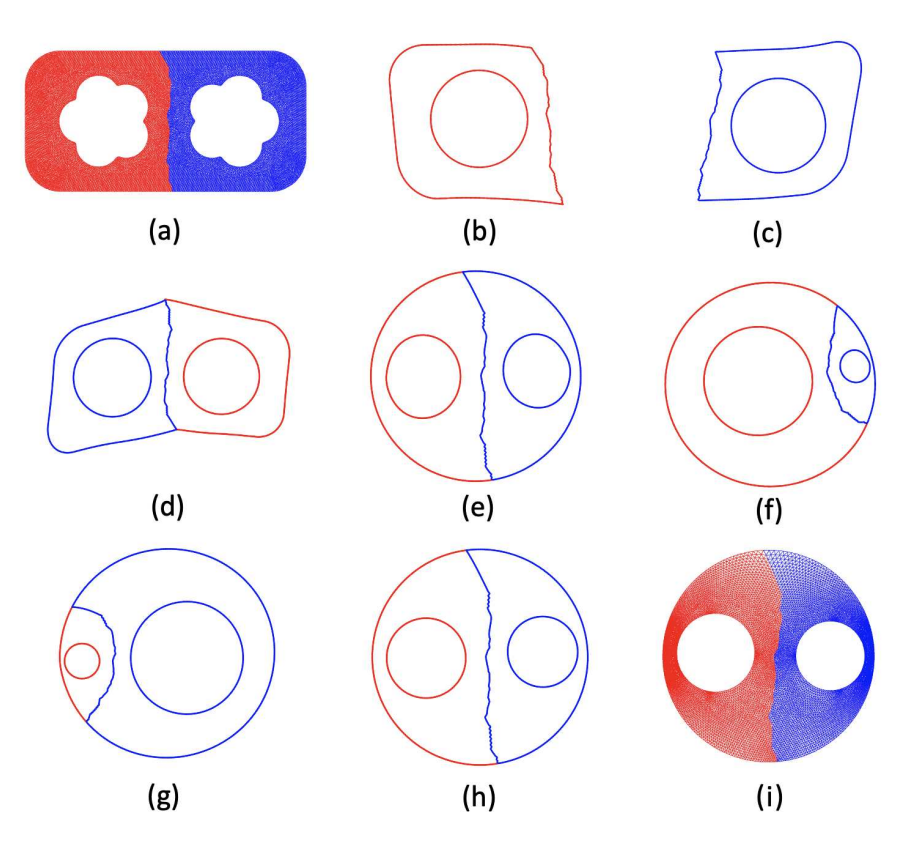


Figure 17. Parameterizing a multiply connected mesh with two very large inner holes using our proposed PGQCM algorithm with multiple cycles of the Koebe's iteration. (a) The input mesh. (b)–(e) One cycle of the Koebe's iteration. (f)–(h) One more cycle of the Koebe's iteration. (i) The final mapping result.

argue that a normalized conformal mapping is very close to the identity map in regions far away from the origin. For surfaces with inner boundaries relatively large and close to the outer boundary, this may not be true, and hence the inner circles may not be well preserved when we transform the outer boundary into a circle in the last step of the parallel Koebe's iteration. Therefore, in this case it may be useful to apply more cycles of the Koebe's iteration. To demonstrate this, we consider a synthetic surface with two large inner holes and perform one cycle of the Koebe's iteration as shown in Figure 17(a)–(e), from which we can see that the two inner boundaries are not very circular (see also Table 7). Applying an additional cycle of Koebe's iteration can enhance the circularity as shown in Figure 17(f)–(h), making the three boundary components very close to perfect circles. Finally, we can solve the Laplace equation to obtain the mapping result in Figure 17(i). Note that although we have performed more than one cycle of the Koebe's iteration in this example, the final errors in Beltrami coefficients of the mapping are still very small (see Table 8).

6. Applications.

6.1. Texture mapping. Our multiply connected quasi-conformal parameterization method can be used for texture mapping on multiply connected open surfaces. More specifically, after

Table 8

Mean absolute error in Beltrami coefficients μ for each submesh in Figure 17.

Submesh	Error e
Submesh 1	0.0097
Submesh 2	0.0108

mapping a given multiply connected 3D surface to a 2D circular domain, we can design the texture on the 2D circular domain freely, and then map the texture onto the mesh using the inverse mapping of the parameterization.

Since conformal parameterizations preserve local geometry, they are commonly used for texture mapping so that the local distortion of the designed texture is small. Similar to [7], we can set the prescribed Beltrami coefficient as 0 in our proposed algorithm and compute a conformal parameterization for texture mapping. An example is given in the top row of Figure 18. Here, we first parameterize a multiply connected human face mesh onto the 2D circular domain conformally using our method. Then, we design a checkerboard texture on the 2D circular domain and map the texture back onto the mesh via the parameterization. It can be observed that the right angles in the checkerboard pattern are well preserved on the human face, which indicates that the local geometry is not distorted.

Moreover, since our method is capable of computing quasi-conformal parameterizations, it grants us more flexibility in the texture mapping design. Specifically, we can prescribe the level of local geometric distortion at any point freely using the input Beltrami coefficient, which allows us to design textures with different visual effects via the quasi-conformal parameterization. An example is given in the bottom row of Figure 18. Note that the orthogonality of the checkerboard texture is well preserved at the nose of the human face, while an angular distortion in the checkerboard pattern can be clearly observed at the chin and the forehead. This demonstrates the possibility of achieving different texture mapping effects using our proposed method.

- **6.2. Remeshing.** Similar to [7], our algorithm can be used to perform surface remeshing. Given a 3D multiply connected open surface, we first parameterize it onto a standard 2D circular domain using our proposed method. Then, we can design a new mesh structure in the circular domain, and finally obtain the remeshed 3D surface with the new mesh structure using the inverse mapping. Two examples are given in Figure 19. In both examples, the remeshing in the circular domain is done using the ddiff and dcircle functions in the DistMesh toolbox [60]. We remark that analogous to the texture mapping application described above, here we can achieve different remeshing effects by using different choices of the Beltrami coefficient in computing the quasi-conformal parameterization.
- 7. Discussion. In this paper, we have developed a novel parallelizable method for computing the global quasi-conformal parameterization of multiply connected surfaces. Given any multiply connected open surface and any prescribed Beltrami coefficient μ , our method computes a quasi-conformal parameterization onto a 2D circular domain in a parallelizable manner. In particular, with the prescribed Beltrami coefficient being $\mu = 0$, conformal parameterizations can be efficiently obtained. When compared to other existing conformal and quasi-conformal parameterization methods for multiply connected surfaces, our proposed method is

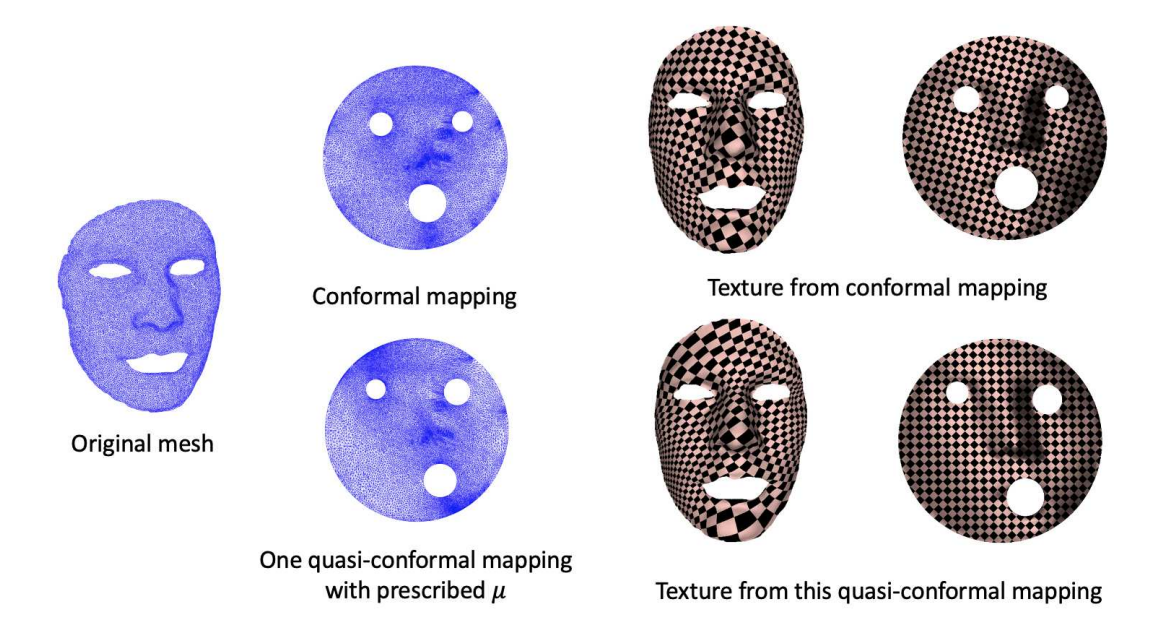


Figure 18. Texture mapping using the conformal and quasi-conformal parameterizations obtained by our proposed algorithm.

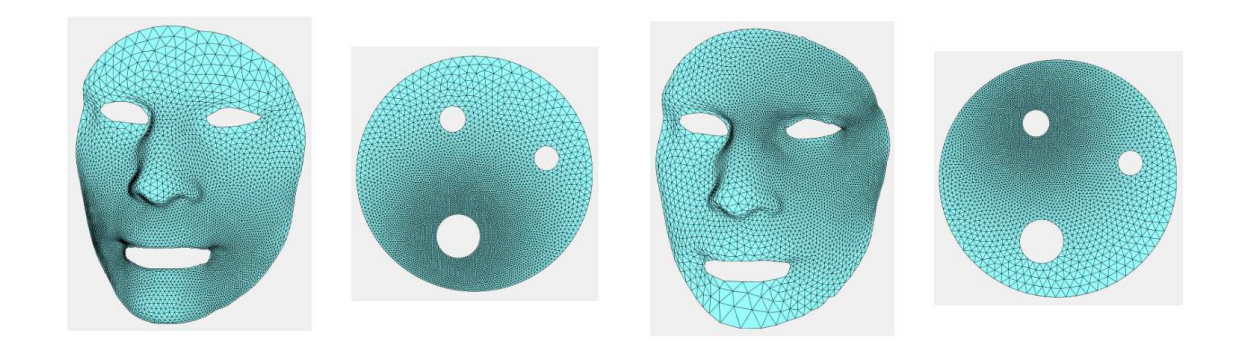


Figure 19. Remeshing a 3D multiply connected open surface using our proposed algorithm.

more advantageous in both efficiency and accuracy.

A known issue of conformal mapping is that the area distortion may be significant [38], and this also happens in the quasi-conformal case [64]. Therefore, it is natural to ask how we can reduce the area distortion of the quasi-conformal parameterization without altering the Beltrami coefficient μ . Similar to [7, 11], it may be possible to search for an optimal automorphism of the unit disk after obtaining the global parameterization $\Phi: \mathcal{S} \to \mathbb{C}$ in the last step in Algorithm 5 such that $f \circ \Phi$ reduces the area distortion of the parameterization. In our future work, we plan to explore different possible measures of the area distortion and optimization methods for improving the performance of the area correction and to develop

methods for reducing the area distortion in a parallelizable manner.

Also, in our experiments, for simplicity we perform the computation using the Parallel Computing Toolbox in MATLAB. Although we can already achieve a significant improvement in the performance when compared to the prior methods, the Parallel Computing Toolbox in MATLAB may not be the best choice for our proposed method. For instance, as mentioned by [11], some of the MATLAB built-in functions, such as fminunc, are not parallelizable under the parallel computing framework of MATLAB, and so MATLAB may not allow us to fully exploit parallelization in some steps of our proposed method. Therefore, we plan to consider other scientific computing software and platforms more specialized to parallel computing. We also plan to explore the use of other fast linear system solvers, such as those in [40, 59], for further improving computational efficiency.

REFERENCES

- L. Ahlfors and L. Bers, Riemann's mapping theorem for variable metrics, Ann. of Math. (2), 72 (1960), pp. 385–404.
- [2] D. An, X. Gu, And S.-T. Yau, Geometric variational framework for computing optimal transportation maps, Math. Comput. Geom. Data, 1 (2022), pp. 1–37.
- [3] S. Angenent, S. Haker, A. Tannenbaum, and R. Kikinis, On the Laplace-Beltrami operator and brain surface flattening, IEEE Trans. Med. Imaging, 18 (1999), pp. 700–711.
- [4] K. ASTALA, T. IWANIEC, AND G. MARTIN, Elliptic Partial Differential Equations and Quasiconformal Mappings in the Plane, Princeton Math. Ser. 48, Princeton University Press, 2009.
- [5] A. I. Bobenko, S. Sechelmann, and B. Springborn, Discrete conformal maps: Boundary value problems, circle domains, Fuchsian and Schottky uniformization, in Advances in Discrete Differential Geometry, Springer, 2016, pp. 1–56.
- [6] E. CHIEN, Z. LEVI, AND O. WEBER, Bounded distortion parametrization in the space of metrics, ACM Trans. Graphics, 35 (2016), pp. 1–16.
- [7] G. P. T. Choi, Efficient conformal parameterization of multiply-connected surfaces using quasi-conformal theory, J. Sci. Comput., 87 (2021), pp. 1–19.
- [8] G. P. T. Choi, H. L. Chan, R. Yong, S. Ranjitkar, A. Brook, G. Townsend, K. Chen, and L. M. Lui, Tooth morphometry using quasi-conformal theory, Pattern Recognition, 99 (2020), 107064.
- [9] G. P. T. CHOI, B. CHIU, AND C. H. RYCROFT, Area-preserving mapping of 3D carotid ultrasound images using density-equalizing reference map, IEEE Trans. Biomed. Engrg., 67 (2020), pp. 1507–1517.
- [10] G. P.-T. Choi, K. T. Ho, and L. M. Lui, Spherical conformal parameterization of genus-0 point clouds for meshing, SIAM J. Imaging Sci., 9 (2016), pp. 1582–1618, https://doi.org/10.1137/15M1037561.
- [11] G. P. T. CHOI, Y. LEUNG-LIU, X. GU, AND L. M. LUI, Parallelizable global conformal parameterization of simply-connected surfaces via partial welding, SIAM J. Imaging Sci., 13 (2020), pp. 1049–1083, https://doi.org/10.1137/19M125337X.
- [12] G. P. T. Choi, Y. Liu, and L. M. Lui, Free-boundary conformal parameterization of point clouds, J. Sci. Comput., 90 (2022), pp. 1–26.
- [13] G. P.-T. Choi and L. M. Lui, A linear formulation for disk conformal parameterization of simplyconnected open surfaces, Adv. Comput. Math., 44 (2018), pp. 87–114.
- [14] G. P.-T. Choi, M. H.-Y. Man, and L. M. Lui, Fast spherical quasiconformal parameterization of genus-0 closed surfaces with application to adaptive remeshing, Geom. Imaging Comput., 3 (2016), pp. 1–29.
- [15] G. P. T. Choi, D. Qiu, and L. M. Lui, Shape analysis via inconsistent surface registration, Proc. Roy. Soc. A, 476 (2020), 20200147.
- [16] G. P. T. Choi and C. H. Rycroft, Density-equalizing maps for simply connected open surfaces, SIAM J. Imaging Sci., 11 (2018), pp. 1134–1178, https://doi.org/10.1137/17M1124796.
- [17] P. T. Choi, K. C. Lam, and L. M. Lui, Flash: Fast landmark aligned spherical harmonic pa-

- rameterization for genus-0 closed brain surfaces, SIAM J. Imaging Sci., 8 (2015), pp. 67–94, https://doi.org/10.1137/130950008.
- [18] P. T. CHOI AND L. M. Lui, Fast disk conformal parameterization of simply-connected open surfaces, J. Sci. Comput., 65 (2015), pp. 1065–1090.
- [19] D. CROWDY, The Schwarz-Christoffel mapping to bounded multiply connected polygonal domains, Proc. Roy. Soc. A, 461 (2005), pp. 2653–2678.
- [20] D. CROWDY, Schwarz-Christoffel mappings to unbounded multiply connected polygonal regions, Math. Proc. Cambridge Philos. Soc., 142 (2007), pp. 319–339.
- [21] D. CROWDY AND J. MARSHALL, Conformal mappings between canonical multiply connected domains, Comput. Methods Funct. Theory, 6 (2006), pp. 59–76.
- [22] L. Cui, X. Qi, C. Wen, N. Lei, X. Li, M. Zhang, and X. Gu, Spherical optimal transportation, Comput.-Aided Des., 115 (2019), pp. 181–193.
- [23] M. Desbrun, M. Meyer, and P. Alliez, Intrinsic parameterizations of surface meshes, Comput. Graphics Forum, 21 (2002), pp. 209–218.
- [24] M. S. Floater and K. Hormann, Surface parameterization: A tutorial and survey, in Advances in Multiresolution for Geometric Modelling, Math. Vis., Springer, 2005, pp. 157–186.
- [25] J. J. GARCIA-LUNA-ACEVES AND S. MURTHY, A path-finding algorithm for loop-free routing, IEEE/ACM Trans. Networking, 5 (1997), pp. 148–160.
- [26] F. P. GARDINER AND N. LAKIC, Quasiconformal Teichmüller Theory, Math. Surveys Monogr. 76, American Mathematical Society, 2000.
- [27] A. GIRI, G. P. T. CHOI, AND L. KUMAR, Open and closed anatomical surface description via hemispherical area-preserving map, Signal Process., 180 (2021), 107867.
- [28] D. Gu, RiemannMapper: A Mesh Parameterization Toolkit, https://www3.cs.stonybrook.edu/~gu/software/RiemannMapper/.
- [29] D. Gu, Stony Brook 3D Scanning Laboratory, https://www3.cs.stonybrook.edu/~gu/software/holoimage/index.html.
- [30] X. Gu, Y. Wang, T. F. Chan, P. M. Thompson, and S.-T. Yau, Genus zero surface conformal mapping and its application to brain surface mapping, IEEE Trans. Med. Imaging, 23 (2004), pp. 949– 958.
- [31] X. Gu and S.-T. Yau, Global conformal surface parameterization, in Proceedings of the 2003 Eurographics/ACM SIGGRAPH Symposium on Geometry Processing, 2003, pp. 127–137.
- [32] S. Haker, S. Angenent, A. Tannenbaum, R. Kikinis, G. Sapiro, and M. Halle, *Conformal surface parameterization for texture mapping*, IEEE Trans. Vis. Comput. Graphics, 6 (2000), pp. 181–189.
- [33] P. Henrici, Applied and Computational Complex Analysis, Vol. 3: Discrete Fourier Analysis—Cauchy Integrals—Construction of Conformal Maps—Univalent Functions, Wiley Classics, John Wiley & Sons, Inc., 1993.
- [34] K. T. Ho And L. M. Lui, QCMC: Quasi-conformal parameterizations for multiply-connected domains, Adv. Comput. Math., 42 (2016), pp. 279–312.
- [35] K. HORMANN, B. LÉVY, AND A. SHEFFER, Mesh parameterization: Theory and practice, in SIGGRAPH '07: ACM SIGGRAPH 2007 Courses, ACM, New York, 2007.
- [36] J. E. HUTCHINSON, Computing conformal maps and minimal surfaces, in Workshop on Theoretical and Numerical Aspects of Geometric Variational Problems, Proceedings of the Workshop held in Canberra, September 24–28, 1990, G. Dziuk, G. Huisken, and J. Hutchinson, eds., Proc. Centre Math. Appl. Austral. Nat. Univ. 26, Australian National University, Centre for Mathematics and Its Applications, 1991, pp. 140–161.
- [37] M. JIN, J. KIM, F. LUO, AND X. GU, Discrete surface Ricci flow, IEEE Trans. Vis. Comput. Graphics, 14 (2008), pp. 1030–1043.
- [38] L. Kharevych, B. Springborn, and P. Schröder, *Discrete conformal mappings via circle patterns*, ACM Trans. Graphics, 25 (2006), pp. 412–438.
- [39] P. Koebe, Über die konforme Abbildung mehrfach zusammenhängender Bereiche, Jahresber. Deutsch. Math.-Verein., 19 (1910), pp. 339–348.
- [40] I. KOUTIS, G. L. MILLER, AND D. TOLLIVER, Combinatorial preconditioners and multilevel solvers for problems in computer vision and image processing, Comput. Vis. Image Understanding, 115 (2011), pp. 1638–1646.

- [41] E. Kropf, X. Yin, S.-T. Yau, and X. D. Gu, Conformal parameterization for multiply connected domains: Combining finite elements and complex analysis, Engrg. Comput., 30 (2014), pp. 441–455.
- [42] R. KÜHNAU, Numerische Realisierung konformer Abbildungen durch "Interpolation," Z. Angew. Math. Mech., 63 (1983), pp. 631–637.
- [43] R. LAI, Z. WEN, W. YIN, X. GU, AND L. M. LUI, Folding-free global conformal mapping for genus-0 surfaces by harmonic energy minimization, J. Sci. Comput., 58 (2014), pp. 705–725.
- [44] K. C. Lam and L. M. Lui, Landmark- and intensity-based registration with large deformations via quasiconformal maps, SIAM J. Imaging Sci., 7 (2014), pp. 2364–2392, https://doi.org/10.1137/130943406.
- [45] J. ŁAWRYNOWICZ AND J. KRZYŻ, Quasiconformal Mappings in the Plane: Parametrical Methods, Lecture Notes in Math. 978, Springer, 1983.
- [46] O. LEHTO AND K. I. VIRTANEN, Quasiconformal Mappings in the Plane, 2nd ed., translated from the German by K. W. Lucas, Grundlehren Math. Wiss. 126, Springer-Verlag, 1973.
- [47] B. LÉVY, S. PETITJEAN, N. RAY, AND J. MAILLOT, Least squares conformal maps for automatic texture atlas generation, ACM Trans. Graphics, 21 (2002), pp. 362–371.
- [48] Y. LIPMAN, Bounded distortion mapping spaces for triangular meshes, ACM Trans. Graphics, 31 (2012), pp. 1–13.
- [49] L. M. Lui, K. C. Lam, T. W. Wong, and X. Gu, Texture map and video compression using Beltrami representation, SIAM J. Imaging Sci., 6 (2013), pp. 1880–1902, https://doi.org/10.1137/120866129.
- [50] L. M. Lui, K. C. Lam, S.-T. Yau, and X. Gu, Teichmüller mapping (T-map) and its applications to landmark matching registration, SIAM J. Imaging Sci.., 7 (2014), pp. 391–426, https://doi.org/10. 1137/120900186.
- [51] L. M. Lui, T. W. Wong, W. Zeng, X. Gu, P. M. Thompson, T. F. Chan, and S.-T. Yau, Optimization of surface registrations using Beltrami holomorphic flow, J. Sci. Comput., 50 (2012), pp. 557–585.
- [52] F. Luo, Combinatorial Yamabe flow on surfaces, Commun. Contemp. Math., 6 (2004), pp. 765-780.
- [53] D. E. MARSHALL, Conformal welding for finitely connected regions, Comput. Methods Function Theory, 11 (2012), pp. 655–669.
- [54] D. E. Marshall and J. A. Morrow, Compositions of Slit Mappings, manuscript.
- [55] D. E. MARSHALL AND S. ROHDE, Convergence of a variant of the zipper algorithm for conformal mapping, SIAM J. Numer. Anal., 45 (2007), pp. 2577–2609, https://doi.org/10.1137/060659119.
- [56] T. W. MENG, G. P.-T. CHOI, AND L. M. LUI, TEMPO: Feature-endowed Teichmuller extremal mappings of point clouds, SIAM J. Imaging Sci., 9 (2016), pp. 1922–1962, https://doi.org/10.1137/15M1049117.
- [57] M. M. S. NASSER, PlgCirMap: A MATLAB toolbox for computing conformal mappings from polygonal multiply connected domains onto circular domains, SoftwareX, 11 (2020), 100464.
- [58] T. C. NG, X. Gu, And L. M. Lui, Teichmüller extremal map of multiply-connected domains using Beltrami holomorphic flow, J. Sci. Comput., 60 (2014), pp. 249–275.
- [59] R. Peng and D. A. Spielman, An efficient parallel solver for SDD linear systems, in Proceedings of the Forty-Sixth Annual ACM Symposium on Theory of Computing, 2014, pp. 333–342.
- [60] P.-O. Persson and G. Strang, A simple mesh generator in MATLAB, SIAM Rev., 46 (2004), pp. 329–345, https://doi.org/10.1137/S0036144503429121.
- [61] V. A. PFLUGER, Ueber die Konstruktion Riemannscher Flächen durch Verheftung, J. Indian Math. Soc. (N.S.), 24 (1960), pp. 401–412.
- [62] U. Pinkall and K. Polthier, Computing discrete minimal surfaces and their conjugates, Exp. Math., 2 (1993), pp. 15–36.
- [63] D. QIU, K.-C. LAM, AND L.-M. LUI, Computing quasi-conformal folds, SIAM J. Imaging Sci., 12 (2019), pp. 1392–1424, https://doi.org/10.1137/18M1220042.
- [64] D. QIU AND L. M. Lui, Inconsistent surface registration via optimization of mapping distortions, J. Sci. Comput., 83 (2020), pp. 1–31.
- [65] R. SAWHNEY AND K. CRANE, Boundary first flattening, ACM Trans. Graphics, 37 (2017), pp. 1–14.
- [66] M. SHAQFA, G. P. T. CHOI, AND K. BEYER, Spherical cap harmonic analysis (SCHA) for characterising the morphology of rough surface patches, Powder Technology, 393 (2021), pp. 837–856.
- [67] E. Sharon and D. Mumford, 2D-shape analysis using conformal mapping, Int. J. Comput. Vis., 70 (2006), pp. 55–75.
- [68] A. Sheffer and E. de Sturler, Parameterization of faceted surfaces for meshing using angle-based flattening, Engrg. Comput., 17 (2001), pp. 326–337.

- [69] A. SHEFFER, B. LÉVY, M. MOGILNITSKY, AND A. BOGOMYAKOV, ABF++: Fast and robust angle based flattening, ACM Trans. Graphics, 24 (2005), pp. 311–330.
- [70] A. Sheffer, E. Praun, and K. Rose, Mesh parameterization methods and their applications, Found. Trends Comput. Graphics Vis., 2 (2006), pp. 105–171.
- [71] Y. WANG, L. M. LUI, X. GU, K. M. HAYASHI, T. F. CHAN, A. W. TOGA, P. M. THOMPSON, AND S.-T. YAU, Brain surface conformal parameterization using Riemann surface structure, IEEE Trans. Med. Imaging, 26 (2007), pp. 853–865.
- [72] O. Weber, A. Myles, and D. Zorin, Computing extremal quasiconformal maps, Comput. Graphics Forum, 31 (2012), pp. 1679–1689.
- [73] T. W. Wong and H.-K. Zhao, Computation of quasi-conformal surface maps using discrete Beltrami flow, SIAM J. Imaging Sci., 7 (2014), pp. 2675–2699, https://doi.org/10.1137/14097104X.
- [74] T. W. Wong and H.-K. Zhao, Computing surface uniformization using discrete Beltrami flow, SIAM J. Sci. Comput., 37 (2015), pp. A1342–A1364, https://doi.org/10.1137/130939183.
- [75] Y.-L. YANG, R. Guo, F. Luo, S.-M. Hu, AND X. Gu, Generalized discrete Ricci flow, Comput. Graphics Forum, 28 (2009), pp. 2005–2014.
- [76] P. YAP, Grid-based path-finding, in Advances in Artificial Intelligence, Canadian AI 2002, Lecture Notes in Comput. Sci. 2338, R. Cohen and B. Spencer, eds., Springer, 2002, pp. 44–55.
- [77] M.-H. Yueh, W.-W. Lin, C.-T. Wu, and S.-T. Yau, An efficient energy minimization for conformal parameterizations, J. Sci. Comput., 73 (2017), pp. 203–227.
- [78] M.-H. Yueh, W.-W. Lin, C.-T. Wu, and S.-T. Yau, A novel stretch energy minimization algorithm for equiareal parameterizations, J. Sci. Comput., 78 (2019), pp. 1353–1386.
- [79] C. P. Yung, G. P. T. Choi, K. Chen, and L. M. Lui, Efficient feature-based image registration by mapping sparsified surfaces, J. Vis. Comm. Image Represent., 55 (2018), pp. 561–571.
- [80] R. ZAYER, B. LÉVY, AND H.-P. SEIDEL, Linear angle based parameterization, in Proceedings of the Fifth Eurographics Symposium on Geometry Processing (SGP 2007), Eurographics Association, 2007, pp. 135–141.
- [81] W. Zeng, L. M. Lui, F. Luo, T. F.-C. Chan, S.-T. Yau, and D. X. Gu, Computing quasiconformal maps using an auxiliary metric and discrete curvature flow, Numer. Math., 121 (2012), pp. 671–703.
- [82] W. Zeng, F. Luo, S.-T. Yau, and X. D. Gu, Surface quasi-conformal mapping by solving Beltrami equations, in Proceedings of the IMA International Conference on Mathematics of Surfaces, Springer, 2009, pp. 391–408.
- [83] W. Zeng, X. Yin, M. Zhang, F. Luo, and X. Gu, Generalized Koebe's method for conformal mapping multiply connected domains, in Proceedings of the 2009 SIAM/ACM Joint Conference on Geometric and Physical Modeling, ACM, 2009, pp. 89–100.
- [84] M. ZHANG, R. GUO, W. ZENG, F. LUO, S.-T. YAU, AND X. GU, The unified discrete surface Ricci flow, Graphical Models, 76 (2014), pp. 321–339.
- [85] X. Zhao, Z. Su, X. D. Gu, A. Kaufman, J. Sun, J. Gao, and F. Luo, Area-preservation mapping using optimal mass transport, IEEE Trans. Vis. Comput. Graphics, 19 (2013), pp. 2838–2847.
- [86] G. ZOU, J. HU, X. GU, AND J. HUA, Authalic parameterization of general surfaces using Lie advection, IEEE Trans. Vis. Comput. Graphics, 17 (2011), pp. 2005–2014.